LRO observations of morphology and surface roughness of volcanic cones and lobate lava flows in the Marius Hills

Samuel J. Lawrence,[1] Julie D. Stopar,[1] B. Ray Hawke,[2] Benjamin T. Greenhagen,[3] Joshua T. S. Cahill,[4] Joshua L. Bandfield,[5] Bradley L. Jolliff,[6] Brett W. Denevi,[4] Mark S. Robinson,[1] Timothy D. Glotch,[7] D. Benjamin J. Bussey,[4] Paul D. Spudis,[8] Thomas A. Giguere,[2,9] and W. Brent Garry[10]

[1] The volcanic domes, cones, sinuous rilles, and pyroclastic deposits of the Marius Hills region of the Moon (~13.4°N, 304.6°E) represent a significant episode of magmatic activity at or near the lunar surface that is still poorly understood. Comparisons between LROC NAC block populations, Mini-RF data, and Diviner-derived rock abundances confirm that blocky lava flows comprise the domes of the Marius Hills. 8 μm features measured by Diviner indicate that the domes are not rich in silica and are not significantly different than surrounding mare materials. LROC observations indicate that some of the dome-building lava flows originated directly from volcanic cones. Many of the cones are C-shaped, while others are irregularly shaped, and local topography and lava eruptions affect cone shape. In general, the cones are morphologically similar to terrestrial cinder and lava cones and are composed of varying amounts of cinder, spatter, and lava. Many of the cones are found in local groupings or alignments. The wide range of volcanic features, from broad low domes to steep cones, represents a range of variable eruption conditions. Complex morphologies and variable layering show that eruption conditions were variable over the plateau.

Citation: Lawrence, S. J., et al. (2013), LRO observations of morphology and surface roughness of volcanic cones and lobate lava flows in the Marius Hills, *J. Geophys. Res. Planets*, *118*, 615–634, doi:10.1002/jgre.20060.

1. Introduction

[2] The region of the Moon known as the Marius Hills comprises a large volcanic complex (~35,000 km², centered at ~13.4°N, 304.6°E) that is situated on a plateau in Oceanus

[1]School of Earth and Space Exploration, Arizona State University, Tempe, Arizona, USA.
[2]Hawaii Institute of Geophysics and Planetology, School of Ocean and Earth Science and Technology, University of Hawaii, Honolulu, Hawaii, USA.
[3]Jet Propulsion Laboratory, California Institute of Technology, Pasadena, California, USA.
[4]Johns Hopkins University, Applied Physics Laboratory, Laurel, Maryland, USA.
[5]Department of Earth and Space Sciences, University of Washington, Seattle, Washington, USA.
[6]Department of Earth and Planetary Sciences, Washington University in St. Louis, St. Louis, Missouri, USA.
[7]Department of Geosciences, Stony Brook University, Stony Brook, New York, USA.
[8]Lunar and Planetary Institute, Universities Space Research Association, Houston, Texas, USA.
[9]Intergraph Corporation, Kapolei, Hawaii, USA.
[10]Planetary Geodynamics Laboratory, NASA Goddard Space Flight Center, Greenbelt, Maryland, USA.

Corresponding author: S. Lawrence, School of Earth and Space Exploration, Arizona State University, Tempe, AZ, USA. (Samuel.lawrence@asu.edu)

Procellarum [*McCauley*, 1967a]. The Marius Hills complex is the largest single concentration of volcanic features on the Moon and includes volcanic domes, cones, rilles, and depressions [*McCauley*, 1967a; *Greeley*, 1971; *Whitford-Stark and Head*, 1977; *Weitz and Head*, 1999]. As such, the Marius Hills represent a significant episode of lunar magmatism at or near the surface thought to have occurred during the Imbrian (~3.3 Ga) to Eratosthenian (~2.5 Ga) [*McCauley*, 1967a; *Whitford-Stark and Head*, 1977; *Heather and Dunkin*, 2002; *Heather et al.*, 2003]. The geologic complexity of this region made it one of the strongest candidates for an Apollo landing, and the Marius Hills remain a high-priority target for future human and robotic precursor exploration, as signified by inclusion among the Constellation Project Regions of Interest [*Karlstrom et al.*, 1968; *Elston and Willingham*, 1969; *Wilhelms*, 1993; *Gruener and Joosten*, 2009; *Lawrence et al.*, 2010a]. Previous studies of the Marius Hills region utilized Earth-based telescope observations, Lunar Orbiter, Apollo, and Clementine data, along with newer data sets from the Kaguya spacecraft and the Moon Mineralogy Mapper (M³) to investigate the morphology and composition of its volcanic features. Here, we use new LRO data to re-examine the geology of the volcanic domes, cones, and related depressions.

[3] The irregular morphology of the volcanic domes in the Marius Hills is unlike most other lunar domes, and their formation is still poorly understood, but is thought to result

from effusive eruptions [*Whitford-Stark and Head*, 1977]. *Head and Gifford* [1980] described the Marius Hills domes as low topographic rises topped with lava flows of a rough texture (Class 7 in their classification schema). Elevated circular-polarization ratios (CPR) derived from Arecibo radar observations of the domes are consistent with blocky lava flows beneath a few meters of regolith [*Campbell et al.*, 2009]. Changes in morphology with elevation on the domes suggest changes in eruption style over time.

[4] *McCauley* [1967a, 1967b] observed variations in volcanic dome morphology and used the slope to define two general classes of volcanic dome, those with low slopes of ~2–3° and those with steep slopes of ~6–7°. Many of the domes have a two-tier morphology wherein the bases have low slopes and the upper portions have steeper slopes. *McCauley* [1967a, 1967b] hypothesized that the change in slopes represented a change in composition over time resulting from magma differentiation and that changes in flow thickness and length might reflect increasing silica content of the lava. Others argued for changes in effusion rates, temperature, and/or crystallization over time [*Whitford-Stark and Head*, 1977; *Weitz and Head*, 1999]. No spectral differences have been observed between domes with low slopes and domes with steep slopes, implying that a change in eruption mechanics is responsible for the variety of dome morphologies rather than a change in composition [*Weitz and Head*, 1999; *Heather et al.*, 2003; *Besse et al.*, 2011]. Based on Clementine multispectral analyses, *Weitz and Head* [1999] and *Heather et al.* [2003] interpreted at least two spectral units comprising the domes including low-Ti and high-Ti basalts, as well as some intermediate-Ti units that were not classified. The authors concluded that the compositions of the domes are not measurably different from the surrounding mare, although the domes are embayed and partly flooded by younger mare basalts [*Whitford-Stark and Head*, 1977; *Weitz and Head*, 1999; *Heather et al.*, 2003].

[5] In addition to the volcanic domes, roughly 50 volcanic cones (also often referred to as "horseshoe"-shaped cones, cinder cones, or spatter cones) typically 1–2 km in diameter were previously observed scattered throughout the Marius Hills complex. These cones occur both on domes and isolated in embaying mare units [*McCauley*, 1967a; *Greeley*, 1971; *Whitford-Stark and Head*, 1977; *Weitz and Head*, 1999; *Heather et al.*, 2003]. Several cones have small associated lava flows that *Whitford-Stark and Head* [1977] proposed as possible evidence for volatile-enriched lava eruptions and pyroclastics and that *Weitz and Head* [1999] suggested were evidence for spatter-style eruptions. The superposition of the cones on top of many domes led *McCauley* [1967a, 1967b] and *Heather et al.* [2003] to propose that the cones are younger than the domes and resulted from a change to a somewhat more viscous but still basaltic eruption style, potentially representing the last stages of volcanism in the Marius Hills. *Weitz and Head* [1999], *Heather et al.* [2003], and *Besse et al.* [2011] all observed spectral differences between the domes and cones in the Marius Hills consistent with a difference in eruption mechanics or lava composition, possibly resulting from terminal-stage volcanism and reflecting an increase in glassy or opaque components produced in pyroclastic and/or spatter (possibly cinder) eruptive materials.

[6] Despite numerous previous analyses, the morphology, composition, and geology of the Marius Hills volcanic constructs (i.e., the volcanic domes and the cones) are still poorly constrained, particularly the 1–2 km cones, which were not previously well resolved. Here, we utilize new data sets from LRO including the Lunar Reconnaissance Orbiter Camera (LROC), the Diviner Lunar Radiometer (Diviner), and the Miniature Radio Frequency Experiment (Mini-RF) to investigate the morphology, distribution, composition, and structure of the numerous volcanic domes, cones, and related depressions in the Marius Hills complex with the ultimate goal of better characterizing the style of regional volcanism that led to the formation of these constructs. In particular, we use morphology as well as surface and near surface structure to assess whether or not these cones are primarily composed of cinder-type pyroclastics. The two LROC Narrow Angle Cameras (NACs) provide detailed images of volcanic domes and cones in the Marius Hills at up to ~0.4 m/pixel [*Robinson et al.*, 2010] and allow determination of block abundances associated with the flanks of selected features. Block abundances reflect the structure and nature of the materials that comprise the dome or cone and are sensitive to modes of geologic origin [*Hartmann*, 1969; *Garvin et al.*, 1981]. The Mini-RF experiment provides information on the radar backscatter properties of specific volcanic features that are used to characterize the surface and subsurface roughness, particularly of the domes and lava flows [*Bussey et al.*, 2010; *Nozette et al.*, 2010; *Raney et al.*, 2010, 2012]. Additional information about thermophysical characteristics that enable estimation of properties such as rock abundance for the domes and lava flows is provided by the Diviner radiometer [*Paige et al.*, 2010; *Bandfield et al.*, 2011]. Diviner also provides information about the bulk silicate mineralogy of the Marius Hills domes and surrounding mare units that are used to investigate compositional differences (or lack thereof) between the Marius Hills domes and the surrounding mare [*Glotch et al.*, 2010; *Greenhagen et al.*, 2010; *Jolliff et al.*, 2011].

[7] Digital Elevation Models (DEMs) created from NAC image pairs [*Tran et al.*, 2010] provide morphometrics (i.e., slopes, heights, and lengths) of specific geologic features, such as lava flows, that provide insight into eruption conditions and magma composition. These parameters are used to characterize the shape and dimensions of specific volcanic constructs and lava flows in the Marius Hills, allowing comparisons to other lunar and terrestrial volcanoes. The LROC Wide Angle Camera (WAC) provides 100 m/pixel scale morphology and morphometry, enabling mapping of the distribution and density of features under uniform lighting conditions and consistent cartographic control [*Robinson et al.*, 2010; *Scholten et al.*, 2012] and providing insight into the regional structure and magma distribution as well as allowing comparison to terrestrial volcanic terrains.

2. Data Sources and Methods

2.1. LROC NAC and Block Populations

[8] Radiometrically calibrated (PDS CDR level) LROC NAC frames of the Marius Hills have pixel scales varying from ~0.4 m (from a low-periapsis portion of the 50 km nominal orbit) to ~1.3 m (from the 220 × 30 km stable orbit)

[Robinson et al., 2010]. LROC NAC right and left image pairs were orthographically corrected and mosaicked in ISIS to make accurate (sub-meter) morphometric measurements of lava flows, volcanic cones, and selected block populations.

[9] The fragmentation characteristics (in particular, the size-frequency distribution) of blocks on planetary surfaces are sensitive to the geologic mode of origin of the population [Hartmann, 1969; Garvin et al., 1981; Cintala et al., 1982]. The results of Hartmann [1967, 1969] suggest that the block size frequency distribution for blocks ejected from impact craters should be different from blocks produced by other processes, such as igneous activity. Fourteen specific regions of geologic importance, specifically, the distal ends of lobate flow features and the summits of cones, were selected for areal block abundance determinations. Coordinates and diameters for each discernible block within a count region were manually determined from map-projected NAC frames; in total, the positions and diameters of over 6800 blocks were digitized. Only blocks at least 1 m in diameter that can be unambiguously identified as a discrete block were included in the digitization process. These block abundance counts not only reflect the jointing and fracturing regime that produced the blocks, but also represent ground truth for select Mini-RF and Diviner observations. The likely sources of uncertainty in the measured block diameters are the misidentifications of blocks and discrepancies between the measured block diameter and the actual block diameter induced by variations in lighting conditions as well as differential burial of blocks of different sizes. To be conservative, all diameter measurements are assumed to have an associated uncertainty of ±1 pixel.

2.2. LROC NAC Digital Elevation Models

[10] The LROC NAC was not designed as a stereo system, but obtains stereo pairs by rolling the LRO spacecraft off-nadir [Lawrence et al., 2009; Robinson et al., 2010; Tran et al., 2010]. NAC image pairs with offset viewing geometries were used to create DEMs of a region in the Marius Hills centered on the Project Constellation Region of Interest. The DEM used in this study has 2.0 m post spacing and an RMS error relative to two LOLA tracks of 4.73 m. DEMs of other lunar volcanic domes were used for comparison to the Marius Hills and include Gruithuisen Gamma (2.0 m post spacing, RMS error relative to one LOLA track of 8.3 m), and Hortensius Phi (5.0 m post spacing, RMS error relative to nine LOLA tracks of 10.3 m). These DEMs are used to make quantitative measurements of volcanic dome slopes, lava flow thickness, and cone slopes and heights.

2.3. LROC WAC

[11] The LROC WAC provides global imaging of the Moon sampled to 100 m/pixel. The WAC is a push-frame camera capturing seven color bands (321, 360, 415, 566, 604, 643, and 689 nm) with a 57 km swath width in color mode and a 105 km swath width in monochrome mode from the 50 km nominal LRO mission orbit [Robinson et al., 2010; Speyerer et al., 2011]. WAC images of the Marius Hills region were mosaicked to create a base map favorable for morphological studies. This basemap was also used to map the distribution and the density of volcanic constructs and characterize their morphology at the 100 m/pixel scale.

The morphologies and distributions of the lava flows and cones, as determined from both LROC NAC and WAC images, were compared to other lunar and terrestrial volcanic constructs in order to assess the style of volcanism that has occurred in the Marius Hills.

[12] The WAC images from adjacent orbits have approximately 50% overlap and 30° stereo angle at the equator. There is nearly complete orbit-to-orbit stereo overlap of the entire Moon, excluding the highest latitudes (i.e., ≥80°). Scholten et al. [2012] computed a digital terrain model at 100 m/pixel (named the LROC WAC Global Lunar DTM 100 m, properly shortened to the "GLD100" model) covering 79°S–79°N with a vertical accuracy of 10 m. The GLD100 product of Scholten et al. [2012] was used in this study to determine of the heights and slopes of volcanic domes and lava flows with diameters greater than 1 km in the Marius Hills region.

2.4. Diviner

[13] Diviner is a nine-channel push-broom mapping radiometer that observes the emitted thermal radiation (seven channels) and reflected solar radiation (two channels) between 0.3 and 400 μm at a spatial resolution of approximately 160×320 m from the 50 km nominal mission orbit [Paige et al., 2010]. In this study, Diviner data were used to produce information about the bulk silicate mineralogy and the areal fraction of rocks on the lunar surface and were used to investigate whether or not the unusual morphology of the Marius Hills lava flows and domes might be a result of a silica-enriched composition, as was originally suggested by McCauley [1967a, 1967b] to explain the observed changes in slope between and among the domes.

[14] Diviner has three spectral bandpass filters centered at 7, 8.25, and 8.55 μm (Channels 3–5) designed to characterize the position and shape of the Christiansen Feature (CF) [Paige et al., 2010]. A polynomial fit to the brightness temperature of these three bands is used to characterize the position of the CF, which is strongly dependent on the degree of silicate polymerization and thus sensitive to key tracers of silicic volcanism, including quartz, silica-rich glass, and alkali and ternary feldspars [Greenhagen et al., 2010]. For compositions that are rich in silica, a spectral parameter called the concavity index is used to characterize the shape of the CF and map relative differences in silica abundance [Glotch et al., 2010, 2011]. Using Diviner data collected from 5 July 2009 to 15 June 2012, we generated maps of the CF position and concavity index in the Marius Hills region to determine the silicate mineralogy and map areas with high silica abundance.

[15] Information from Diviner channels 6 (13–23 μm), 7 (25–41 μm), and 8 (51–100 μm) provides the means to estimate areal rock abundance with a spatial resolution of 500 m/pixel following the procedures outlined in Bandfield et al. [2011]. Data from each channel were binned at 32 pixels/degree in 10 one hour increments of local time from 1430 to 0530. The relatively warm rocks and cold regolith can be distinguished from the cooler surrounding regolith using multiple wavelength measurements and the surface rock fraction can be derived [Christensen, 1986; Colwell and Jakosky, 2002; Nowicki and Christensen, 2007; Bandfield and Edwards, 2008; Bandfield, 2009]. Using rock abundances derived from the Diviner data sets,

we determined the average model rock abundance for the Marius Hills volcanic constructs, which can be compared to NAC boulder counts and Mini-RF surface roughness in order to, in particular, quantify the blockiness of the lava flows that comprise the domes. The data product used in this study is an estimate of the surface rock exposure areal fraction (on a scale of 0–100%).

2.5. Mini-RF Radar

[16] The Miniature Radio Frequency (Mini-RF) instrument uses a hybrid polarimetric architecture to measure the lunar surface backscatter characteristics and is discussed in detail in *Nozette et al.* [2010]. It transmits a left circular polarized signal and receives coherently H and V orthogonal polarizations as well as the phase signal between the polarizations. Mini-RF acquired observations in one of two radar frequencies, S-band (12 cm) or X-band (4 cm) band with two resolution modes: baseline (150 m) and zoom (30 m). The unique architecture of Mini-RF enables the determination of all four of the Stokes parameters of the backscattered field, referred to as S_1, S_2, S_3, and S_4 [*Raney*, 2006; *Nozette et al.*, 2010; *Raney et al.*, 2010]. Data products from the Mini-RF instrument are useful for investigating the surface and near-subsurface properties of the surface to a depth of approximately 10 times the radar wavelength [*Campbell and Campbell*, 2006; *Neish et al.*, 2011] and are used in combination with NAC-derived block populations and Diviner-derived rock abundances to investigate the assertions of *Head and Gifford* [1980] and *Campbell et al.* [2009] that the domes comprise rough, blocky lava flows. Two particularly useful data products are the S_1, which represents the total radar backscatter and is a commonly used proxy for surface roughness in planetary radar investigations, and the Circular Polarization Ratio (CPR), which is particularly sensitive to the presence of blocks on the surface and within the near-subsurface [*Raney et al.*, 2010]. CPR is defined as the ratio of the backscattered power in the same-sense (SC) relative to opposite-sense (OC) polarizations. To calculate the CPR of the received signal, it is necessary to calculate the total power returned in the same polarization as was transmitted (SC = $S_1 - S_4$) relative to the total power returned in the opposite polarization (OC = $S_1 + S_4$). Data products presented here are derived from calibrated and map-projected Mini-RF S-band zoom observations.

[17] Another radar parameter leveraged here is referred to as an *m-chi* decomposition, which is an analysis tool that while widely used in terrestrial radar analyses has only recently been implemented for radar analyses of the lunar surface [*Cahill et al.*, 2012; *Raney et al.*, 2012]. Briefly, *m-chi* decompositions depend on upon quantifying two variables (*m* and *chi*, referring to two parts of a returned signal), which when used together uniquely characterize the backscattering characteristics of the observed scene [*Raney et al.*, 2012]. As described in *Raney et al.* [2012], the depolarized portion of the returned signal is quantified with *m*, which is the degree of polarization, and is defined as

$$m = \frac{\left(S_2^2 + S_3^2 + S_4^2\right)^{1/2}}{S_1} \quad (1)$$

[18] The degree of circularity, or sin2χ, is defined as

$$\sin 2\chi = -S_4/mS_1 \quad (2)$$

[19] The polarized portion of the signal is quantified by *chi*. *Chi* includes measurements of randomly polarized returns (i.e., volume scattering, *vs*) as well as single (e.g., Bragg scattering surfaces, *bs*) and double bounce (e.g., dihedral surfaces, *db*) polarized backscatter returns from the lunar surface. Double bounce (*db*), volume scattering (*vs*), and single bounce backscatter (*bs*) are described by the following equations within an RGB image:

$$R = db = [mS_1(1 + \sin 2\chi)/2]^{1/2} \quad (3)$$

$$G = vs = [S_1(1 - m)]^{1/2} \quad (4)$$

$$B = bs = [mS_1(1 - \sin 2\chi)/2]^{1/2} \quad (5)$$

[20] The *m-chi* is a complementary product to CPR that permits a rigorous quantification of surface scattering properties and does not need to be combined or overlaid on S_1 maps for morphological information in the same manner often required for CPR maps [*Raney et al.*, 2012].

3. Results

[21] The geologic features in the Marius Hills are diverse and include volcanic cones, associated lava flows, domes, and sinuous rilles (Figure 1). We completed a survey of the volcanic domes and cones in the Marius Hills region using data from the first 3 years of LRO operations, with an emphasis on morphology. Particular emphasis is placed on the 1–2 km in diameter volcanic cones that previous sensors could not easily resolve, but which are an important part of the volcanic processes in the Marius Hills complex. First, we examine the morphology of more than 150 volcanic domes and 90 cones in the Marius Hills in order to better characterize the style of volcanism that has occurred. Block populations and surface roughness of selected domes, cones, and lava flows are used to further characterize the structure and physical properties of the volcanic materials at the surface. Finally, we analyze the composition of the volcanic constructs and lava flows.

3.1. Morphology and Morphometry

3.1.1. Volcanic Domes

[22] Historically, the large volcanic constructs in the Marius Hills have been interpreted as low shields [*Guest and Murray*, 1976], or more commonly, low domes and steep-sided domes [*McCauley*, 1967a; *Whitford-Stark and Head*, 1977], formed by effusive eruptions. With observations made from LROC images, the characterization of these Marius Hills volcanic domes can be refined in order to more completely describe the morphology of these features. Our observations are generally consistent with those of previous works:

[23] (1) In general, the domes are topographic rises with irregular surfaces.

[24] (2) The domes have irregular outlines and range in size from 2 km to tens of kilometers in diameter, with most being between 5 and 6 km.
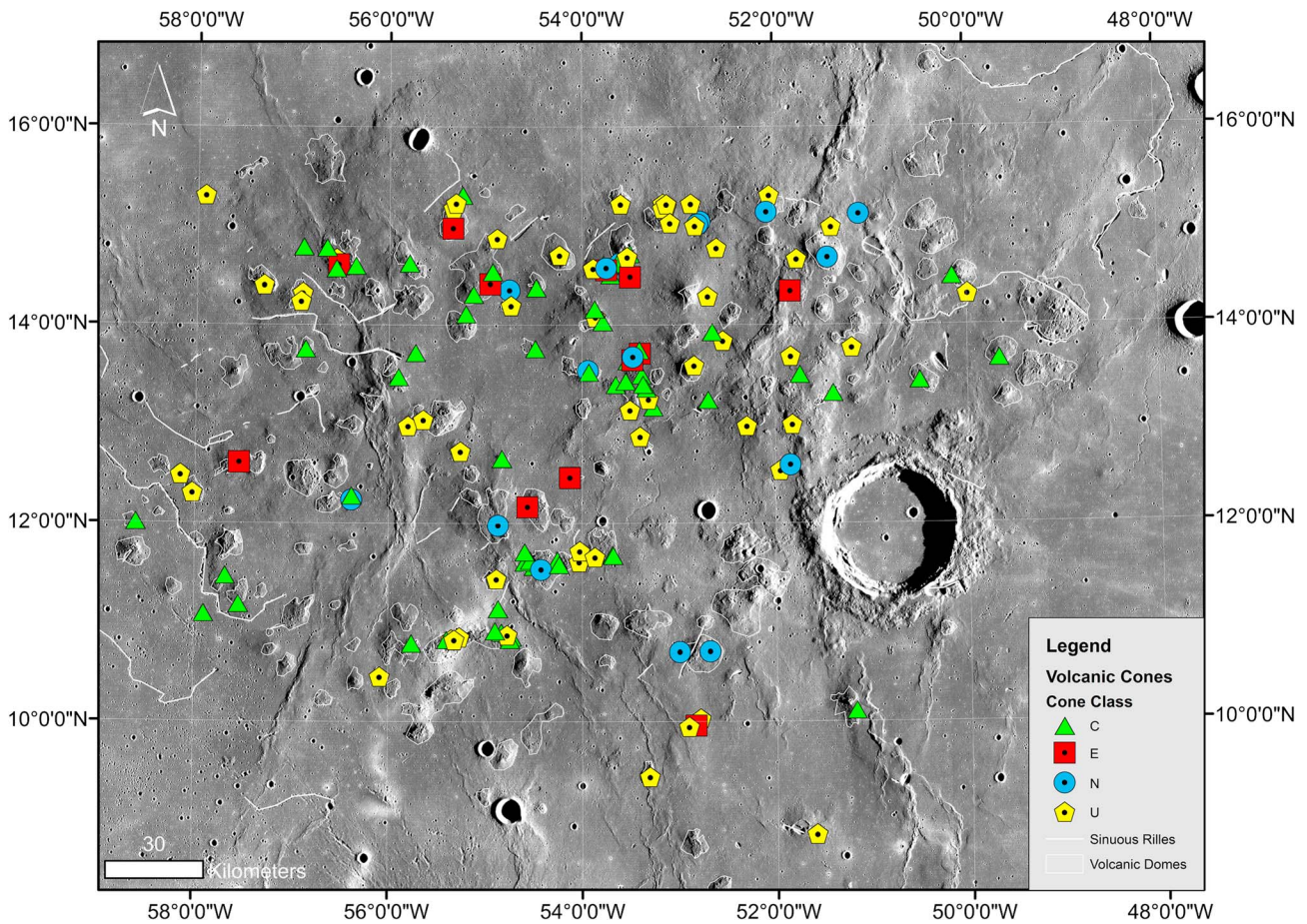
Figure 1. Regional map of volcanic features in the Marius Hills, charted using an LROC Wide Angle Camera base map. Locations and classifications of cones, volcanic domes, and sinuous rilles are highlighted.

[25] (3) Some domes are geographically associated with sinuous rilles, rille-like features, collapse pits, and/or graben (Figures 2a and 2g).

[26] (4) Some domes are associated with volcanic cones and/or vents (Figures 2b and 2h).

[27] (5) Some domes are comprised of distinct and often overlapping lava flows, which in several cases have been measured at up to 5 km long (Figures 2c and 2i). Some of these flows radiate from volcanic vents or cones whereas others do not have obvious sources. The distal ends of the lava flows are commonly lobate, and, where sufficient topographic data allow measurement, have heights of more than 30 m. The ends of flow lobes are steep and covered with blocks. Topographic profiles of the lava flows indicate that the steepest slopes, measured up to 17°, are found at their distal ends (Figure 3). These lava flows form irregular constructs with average slopes measured up to 10°. Some lava flows have combined to form plateaus with relatively flat and smooth tops (Figures 2d and 2j); others are concave, suggesting collapse of the central region and/or inflation of the margins (Figures 2e and 2k).

[28] (6) Some domes are low and broad, lack obvious vents, and may be degraded lava flows (Figures 2d and 2l). Slopes on the flanks of these domes are a few degrees (≤3°).

[29] (7) Many domes have a two-tiered morphology consisting of a low, broad base and superposed irregular lava

flows or lava shields. These constructs have variable slopes, and the slopes are generally lower near the base and steeper toward the center.

[30] Younger mare flows embay the Marius Hills domes and cones; in some cases only the uppermost portions of the original features remain visible. Therefore, the observed volcanic domes and cones do not necessarily reflect the original boundaries. Other factors have also affected the volcanic constructs since their formation including modification during the compressive stresses associated with wrinkle ridge formation. Several wrinkle ridges cross through the Marius Hills, primarily on a SSE-NNW trend, and previously were observed to have modified sinuous rilles and volcanic constructs in the region [*Lawrence et al.*, 2010b].

[31] When used to describe lunar geologic features, the term "dome" historically has referred to a topographic rise of presumed volcanic origin that has slopes up to 5°, has a diameter less than 30 km, and is distinct from its surroundings [*Smith*, 1973; *Head and Gifford*, 1980]. The Marius Hills domes are consistent with this definition. In a global survey of volcanic domes, *Head and Gifford* [1980] noted the unique nature of the Marius Hills constructs. Figure 4 compares a representative dome in the Marius Hills region, the mare dome Hortensius Phi, and the silicic dome Gruithuisen Gamma. In contrast to the other lunar domes,
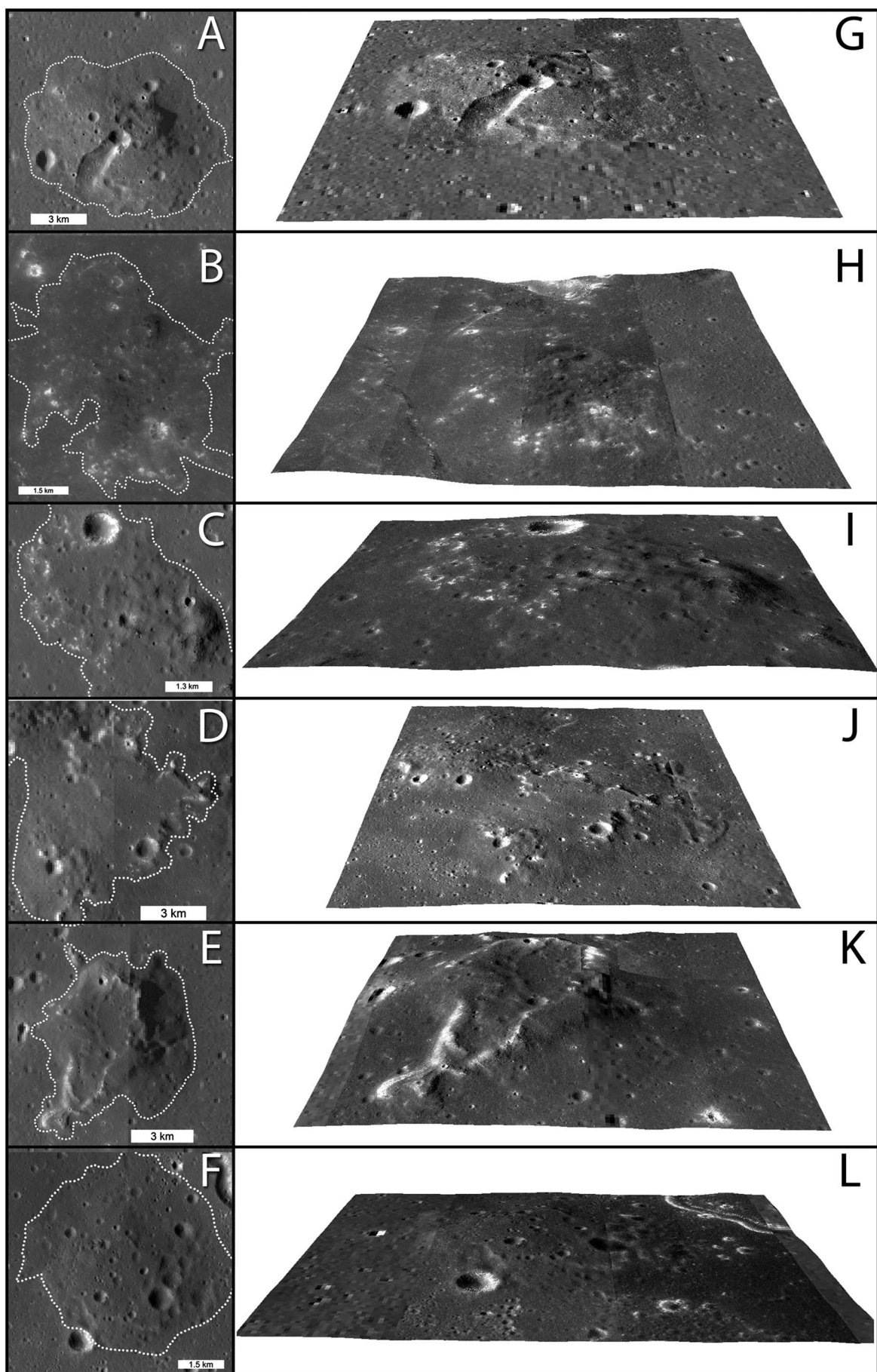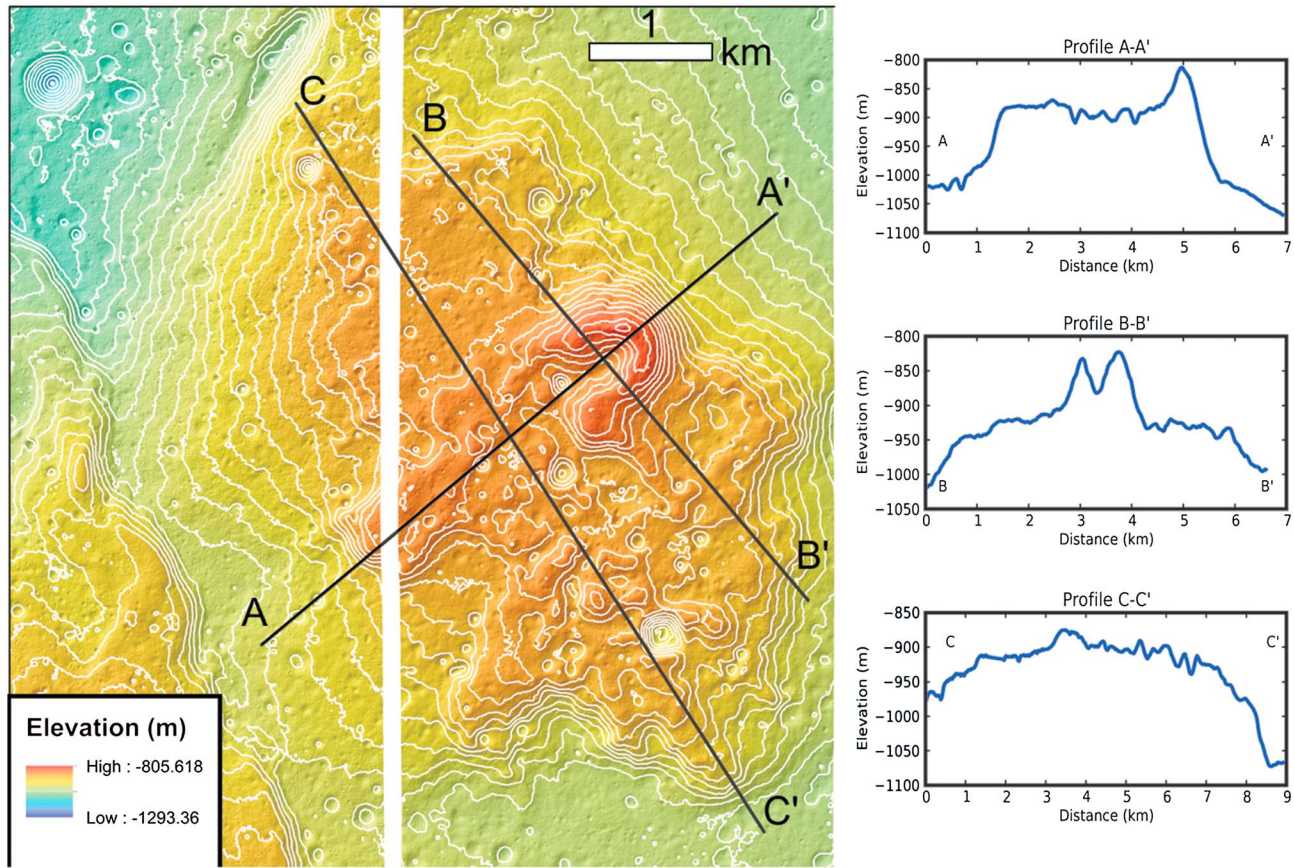
Figure 2.

Figure 3. Digital Elevation Model (5 m contour intervals) derived from LROC NAC images of a volcanic dome with cone in the Marius Hills near the Constellation Program Region of Interest. Representative profiles across the lava flows are reproduced on the right.

the Marius Hills domes have smaller diameters and lower relative heights.

3.1.2. Volcanic Cones

[32] Using LROC NAC and WAC images, we identified 93 volcanic cones in the Marius Hills region, which is higher than the numbers previously reported (46 reported by *Weitz and Head* [1999]; 59 reported by *Whitford-Stark and Head* [1977]). For example, in areas such as the center of the Marius Hills plateau in Figure 5 (centered at 13.45°N, 306.55°E), we identified 11 cones, of which no more than three cones were previously recognized [*Whitford-Stark and Head*, 1977; *Weitz and Head*, 1999; *Heather et al.*, 2003]. An additional 56 constructs were identified that may also be cones, but owing to degradation and/or unfavorable illumination conditions, cannot be identified unambiguously, and are here included for completeness and as potential targets for future robotic and human exploration. We summarize our observations of the Marius Hills cones using the following classes to differentiate between different cone morphologies:

[33] *C-class cone* (*C-shaped*): The C-shaped cones (n = 64) are often the largest and most easily recognized features. The bases of these cones are measured as between 0.5–4 km in diameter. For comparison, terrestrial cinder cones may be a few hundred meters to 2.5 km in diameter depending on eruption conditions [*Wood*, 1979; *Wilson and Head*, 1981], and the majority of the Marius Hills cones also fall within this range. The Marius Hills cones have smooth flanks with relatively constant slope, also similar to terrestrial cinder cones. However, unlike terrestrial cinder cones, the Marius Hills cones have lower flank slopes. Terrestrial cinder cones have flanks slopes near the angle of repose (~30°), at least when mass wasting has not resulted in significant migration of material [*Porter*, 1972; *McGetchin et al.*, 1974; *Wood*, 1980]. In contrast, the flank slopes of the Marius Hills cones are observed as less than 17°, as determined from shadow lengths and NAC-derived DEMs. Despite lower flank slopes, the C-class cones have morphologies reminiscent of terrestrial cinder cones as described in *Porter* [1972], *Wood* [1979,

Figure 2. Examples of volcanic domes (approximate boundaries dotted lines) in the Marius Hills. (a) Portion of a volcanic dome with associated rille-like feature or collapse feature; NAC frame M135568666. (b) Portion of a volcanic dome with associated volcanic cone and lava flows; NAC frame M111958993. (c) Portion of a volcanic dome with distinct lobate lava flows NAC frame M1509870879. (d) Portion of a volcanic dome with plateau formed by lava flows NAC frame M120182106. (e) Concave volcanic dome NAC frame M150897982. (f) Low volcanic dome (approximate boundary dotted line); NAC frame M150850588. (g–l) Corresponding perspective views of volcanic domes (a–f) generated using GLD100 dataset and WAC base map. 2X vertical exaggeration; north toward top.
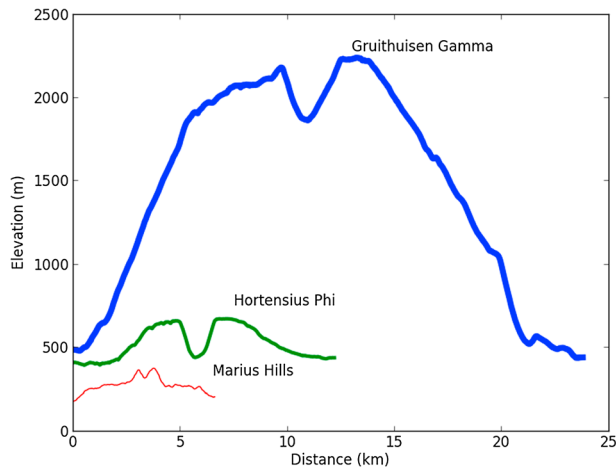
Figure 4. Topographic profiles of Gruithuisen Gamma (a non-mare, silicic dome), Hortensius Phi (a mare dome), and a representative Marius Hill volcanic dome with cone. Profiles were extracted from LROC NAC DEMs of each feature.

1980], and *Weitz and Head* [1999]. *Head* [1975] also noted their similarity to terrestrial composite cones, constructs built from layers of pyroclastic materials and lava flows.

[34] The distinctive C-shape of these cones results from a gap that is commonly associated with at least one lobate lava flow. The point of highest topography along the cone rim is opposite the gap and the rim angles down toward the gap. Any associated lava flows radiate from the central region of the cone to form a volcanic dome (e.g., Figure 2b). Some cones, however, are standalone features completely embayed by younger mare, and any associated domes have been buried (e.g., Figure 6c). The C-class cones often have a local cluster of meter-scale blocks or fractured material on the flanks or associated with the summit crater as well as discrete, coherent layered materials or aligned blocks in their flanks (e.g., Figures 6a, 6d and 7) . This layering was suggested by *Weitz and Head* [1999] for one cone, but is now confirmed. These layers, particularly in the case of Figure 6d, dip downslope and follow the path of lava flows that once erupted out of the cone.

[35] Gaps in individual C-class cones generally coincide with regional downhill slopes (Figure 8). However, some C-class cones are clustered in groups or alignments (Figure 9), and
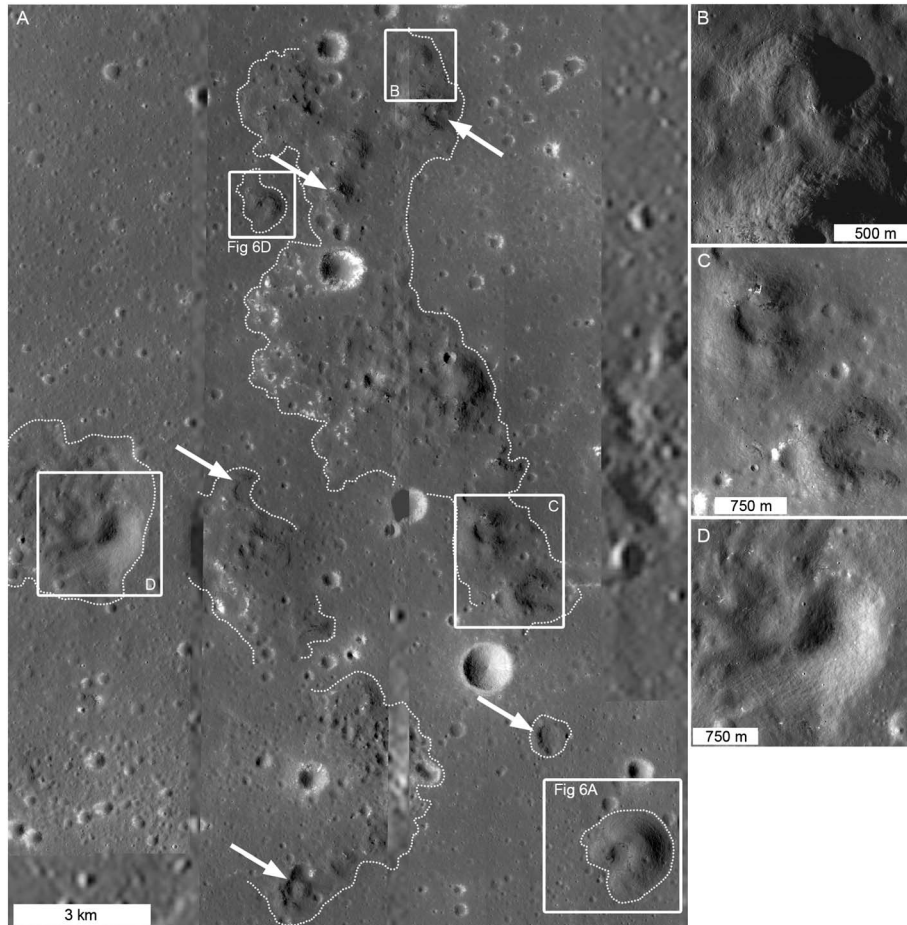
Figure 5. (A) Approximately 297 km^2 region (center at 13.45°N, 306.55°E) near the center of the Marius Hills volcanic complex. Approximate boundaries of volcanic flows and cones are outlined (white dotted) on NAC/WAC mosaic resampled to 0.5 m pixel scale. At least 11 volcanic cones (callouts) and possible cones (arrows) are observed in this area for a local density of 0.037 features/km^2. (B) C-class cone (NAC frame M133180167). (C) Pair of C-class cones (NAC frame M120202440). (D) C-class cone (NAC frame M129642302).
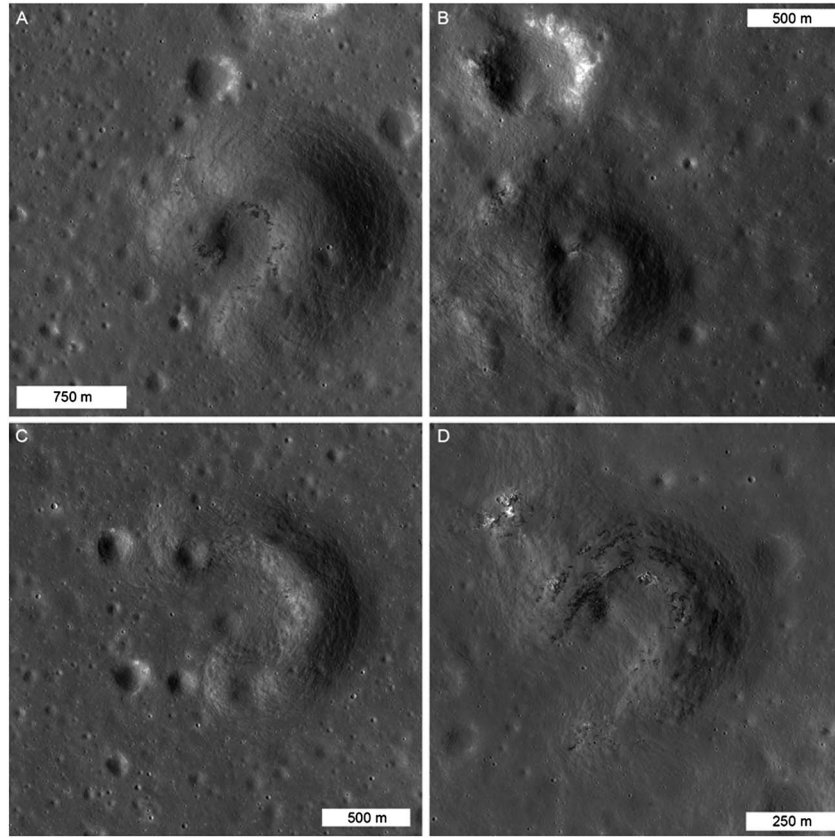
Figure 6. Representative examples of Marius Hills C-class cones. (A) A 1.8 km diameter cone with gap located at 13.17°N, 306.74°E; NAC frame M166195459. (B) A 1.0 km diameter cone with gap located at 11.14°N, 305.13°E; NAC frame M135548319. (C) A 1.3 km diameter cone with gap located at 14.78°N, 303.11°E is embayed by younger mare; NAC frame M135561817. (D) An 800 m diameter cone with gap located at 13.64°N, 306.48°E shows distinct and coherent layers; NAC frame M150870879.

gaps in grouped cones usually occur in different directions and are not always in alignment with local and regional topographic contours. In these cases, the orientation of gaps may result from "obstacle" effects created by the neighboring cones (Figures 8a–8d insets).

[36] To summarize, C-class cones have the following characteristics:

[37] (1) The feature is distinct from its surroundings and has a sharp contact with surrounding materials.
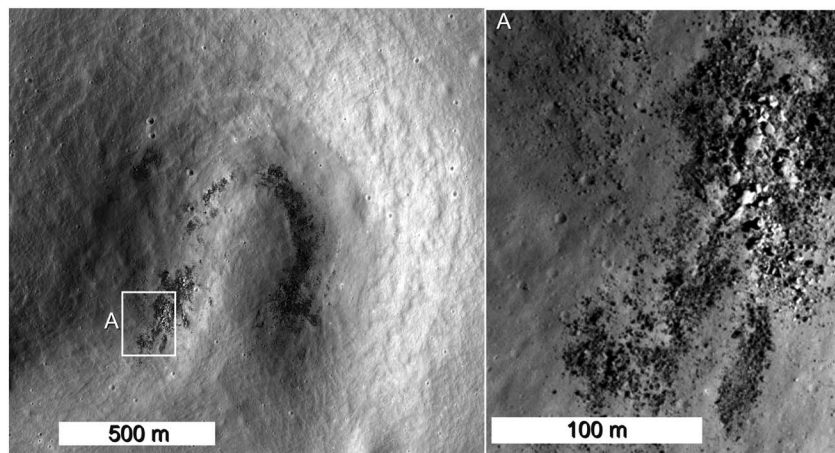
Figure 7. Example of layering in a Marius Hills C-class cone located at 13.25°N, 307.31°E associated with dense abundances of blocks at the summit. Inset (A) is a region where blocks are fracturing from exposed, discrete layers (NAC frame M175623937).
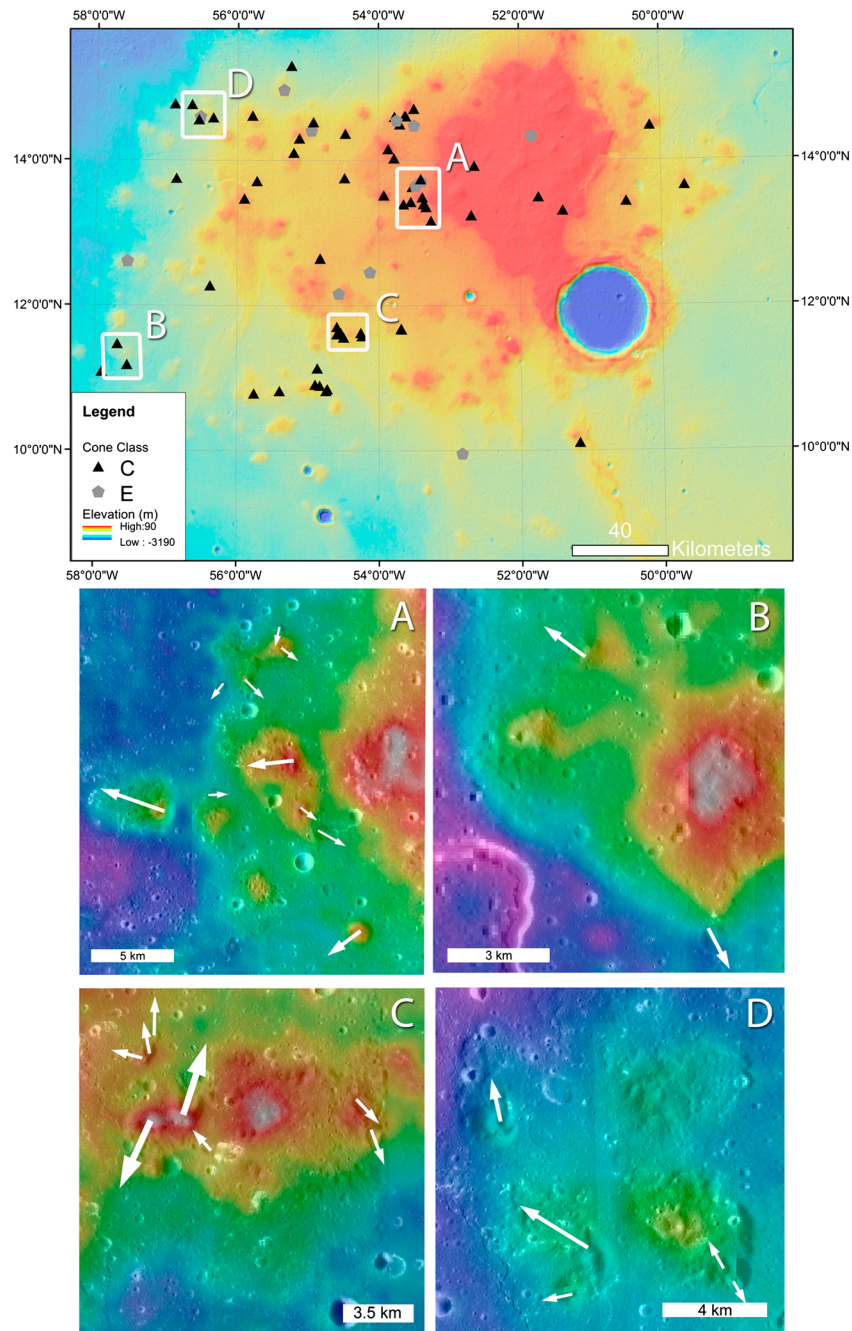
Figure 8. The GLD100 Digital Elevation Model (DEM) of the Marius Hills region; locations of C- and E-class cones are highlighted. Arrows in (A–D) insets indicate the directions of gaps in the C-shaped cones within the Marius Hills region; arrows point away from the cone. White areas in insets are the areas with highest elevations within inset; purple areas have the lowest relative elevations.

[38] (2) The cone rim is topographically higher than the immediate surroundings and relatively higher than impact craters of the same diameter.

[39] (3) These features are less than 4 km in diameter at the base, and most are between 0.5 and 2 km.

[40] (4) Exterior flank slopes are relatively steep (measured up to 16°), and the surfaces themselves are smooth at the meter-scale except for the occasional boulder field or blocky layer at or near the summit (Figure 7).

[41] (5) The cone walls form a partial ellipse, with a gap on one side of the cone, forming a C-shape. Often there are associated lava flows or flow-like morphologies outside the cone.

[42] (6) The point of highest topography in the cone rim is approximately opposite the gap in the ellipse.

[43] (7) Cones may exist individually or in clusters and aligned groups (Figures 8 and 9).

[44] (8) The gap of individual cones is often oriented in the downhill direction (but not always).
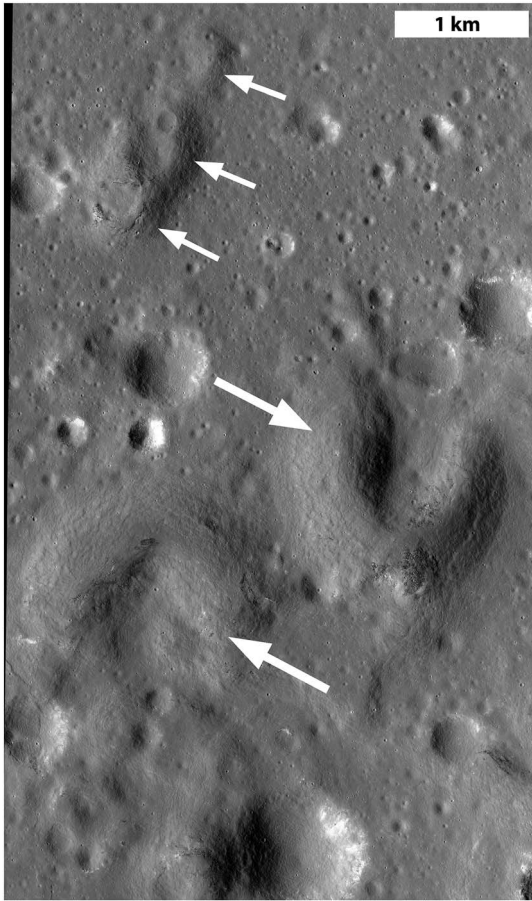
Figure 9. Example of five grouped and aligned C-class cones (white arrows) centered at 11.65°N, 305.41°E. Gaps in grouped cones can occur in different directions. Grouped cones can have intersecting bases and cone walls. (NAC frame M150877632)

[45] *E-class cone* (*Elongate*): These cones (*n* = 12) are morphologically similar to C-class cones, but more elongate in plan view (Figure 10). Like the C-class cones, these cones have a gap containing distinct lava flow channels indicating flow direction. The point of highest topography along the cone rim is roughly opposite the gap. These cones represent a small subset of volcanic cones that have an elongated shape.

[46] *N-class cone* (*No Gap*): These cones (n = 17) have a subcircular to elongate summit crater without the well-developed gap associated with the C-class cones (Figure 11). Like C- and E-class cones, the exterior slopes are relatively steep and smooth, except for the occasional exposed boulder field or blocky layer.

[47] *U-class construct* (*Uncertain cones*): U-class constructs (n = 55) are positive relief features 0.5–4 km in diameter, same as Marius Hills cones, that are not easily distinguished from mantled impact craters, degraded lava flow fronts, or other lunar geologic features (Figure 12). The boundaries of U-class constructs are difficult to distinguish from the surroundings. The flank slopes of several U-class constructs, as measured from shadow lengths, range from a few degrees to 16°, same as the Marius Hills cones. However, due to degradation (and/or illumination), we cannot positively identify these features as volcanic cones. For example, Figure 12b shows a C-shaped construct that may be either a heavily embayed C-class cone or an impact crater draped with mare basalt.
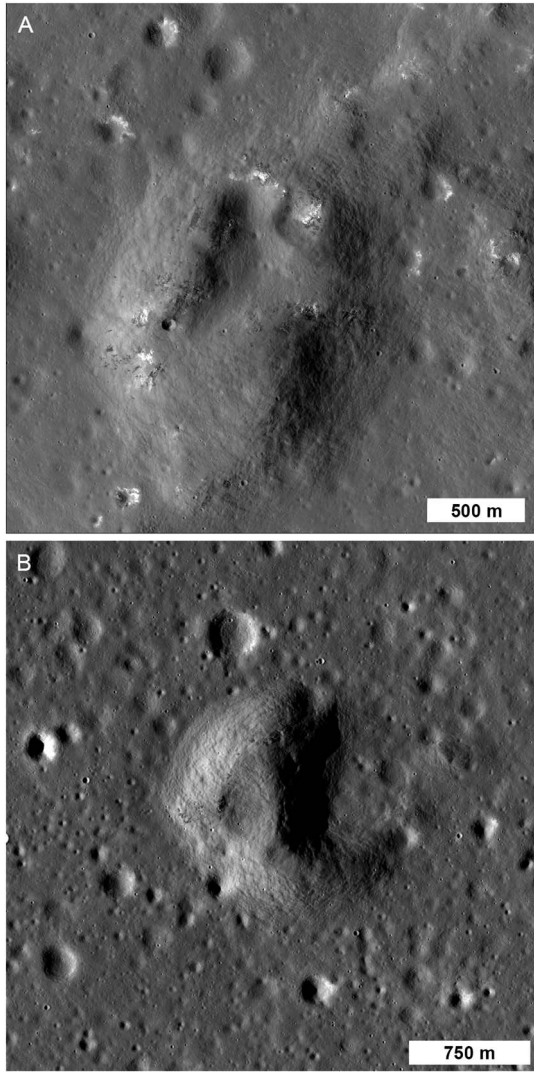
3.2. Block Abundances and Surface Roughness

[48] Block populations and surface roughness are related to the physical properties of volcanic materials and the formation of the domes, lobate lava flows, and cones. Visual inspection of volcanic domes and cones in the Marius Hills region revealed local areas with higher than average abundances of blocks at the resolution of the LROC NAC. Many of the blocks on cones are associated with, and presumably fractured from, discrete rock layers evident at the
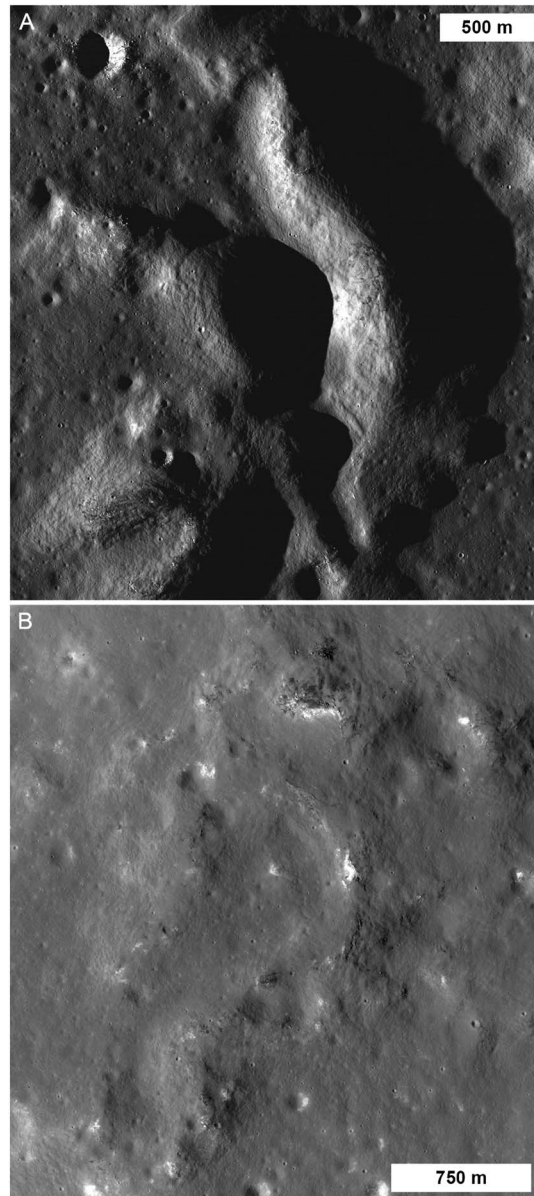
Figure 10. Examples of Marius Hills E-class cones. (A) Elongate (up to ~2.5 km long) cone located at 14.61°N, 303.47°E, with a smaller (~1.2 km diameter) C-class cone adjacent to the SW (NAC frame M133200522). (B) Elongate (up to ~2.3 km long) cone located at 9.96°N, 307.17°E (NAC frame M104862938).

625

Figure 11. Examples of Marius Hills N-class cones: (A) ~1.9 km diameter cone with a poorly defined gap located at 14.67°N, 308.56°E, (NAC frame M150857331). (B) Approximately 1.4 km diameter cone with a poorly defined gap located at 14.35°N, 305.25°E (NAC frame M102515241).

relatively steep slopes, where regolith formation has not obscured blocks. Analysis of the size spectrum of the block populations on the cones and lobate lava flows indicates that the blocks on the lobate lava flows are smaller and have more uniform sizes, than the block populations associated with the volcanic cones, reflecting a difference in origin and mechanical history.

[50] The observed smaller average size of blocks at the ends of the lobate lava flows is consistent with terrestrial observations indicating that the size of primary blocks associated with volcanic vents in high viscosity regimes decreases as distance from the central vent increases [*Anderson et al.*, 1998].

[51] The terminal ends of lobate lava flows and the local block populations on volcanic cones have enhanced double bounce (*db*) and volume (*vs*) scattering at the Mini-RF S-band (12.6 cm) wavelengths relative to the surrounding terrain, consistent with the blocks observed on these constructs in LROC NAC images (Figure 13). In contrast, surrounding mare surfaces exhibit predominantly single bounce scattering, suggesting smooth surfaces scaled to the wavelength being used. Figure 13 shows a representative C-class cone with lobate lava flows emanating through the distinctive gap in the cone. The distal ends of the lobate flows and the summit of the volcanic cone (shown in image insets) have discernible surface block populations that were characterized using LROC NAC images (Table 2). The image insets are locations where block populations were quantified (Table 2). Enhanced radar returns relative to the surrounding terrain are observed for each of the lobate flows; the summit of the cone (Area "e"), which has the largest blocks, also has the highest CPR value. Radar backscatter enhancements are consistently noted at the distal ends of lobate lava flows and volcanic cones with dense block populations. However, the entire portion of each dome does not display enhanced radar backscatter relative to the surrounding terrain, indicating that Mini-RF does not fully penetrate the regolith to reach the lava flows beneath. These findings are also generally consistent with the results of *Campbell et al.* [2009].

[52] Diviner-derived rock abundances, like the NAC-derived block populations and Mini-RF surface roughness, also indicate that the lava flows and domes are rougher and blockier than the surrounding mare. The volcanic domes in the Marius Hills region in the Diviner parameter space have areal rock abundances of $0.9 \pm 0.3\%$. For comparison, the small, fresh impact craters in Oceanus Procellarum typically produce abundant blocks and have areal rock abundances of >10% in the near-rim ejecta blanket, making the ejecta of small fresh impact craters the "blockiest" surfaces in the Marius Hills region, at least in terms of areal exposure of blocks larger than 1 m in diameter. The Marius Hills domes are significantly less blocky than these fresh impact craters, but the Marius Hills domes are blockier than the surrounding mare, which has a rock abundance of $0.4 \pm 0.1\%$, as well as the global areal rock abundance, which is 0.3% [*Bandfield et al.*, 2011]. Although much higher local block abundances are clearly present on parts of domes and cones (as is readily apparent in Figures 6 and 7), these block populations are typically present in discrete locations significantly smaller than the Diviner rock abundance data sampling.

0.5 m scale. Blocks as large as 28 m in diameter were identified on some cones. Blocks are also exposed on the distal ends of the lobate lava flows associated with the volcanic domes in the Marius Hills region. The block populations on the ends of the lava flows do not have associated impact craters, indicating that block occurrences are endemic to these landforms and not erratic blocks produced by impact processes. The average and maximum sizes of the blocks associated with the volcanic cones are larger than those on the lava flows (Table 1).
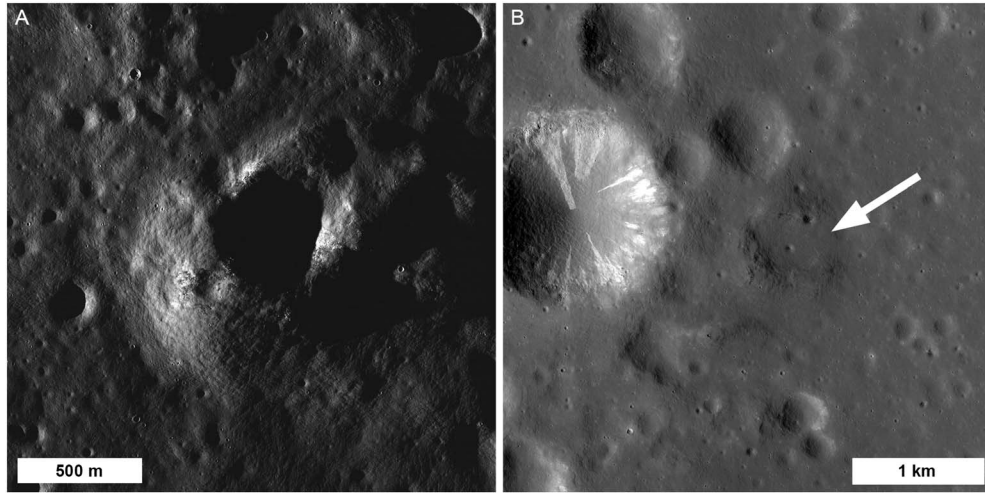
[49] To facilitate comparisons between our new block counts and previous investigations, we followed the approach of *Hartmann* [1969], who used the slope, *b*, of a power-law function fit to the reverse cumulate distribution of the block population to characterize the size spectrum of a block population (results reported in Table 1). In NAC images, the largest abundances of blocks associated with volcanic constructs are found on slopes at the distal ends of lobate lava flows and on portions of the volcanic cones. These are locations with

Figure 12. Examples of Marius Hills U-class constructs. (A) Cone-like topographic feature located at 14.31°N, 304.88°E, with unusual summit crater morphology (NAC frame M148523347). (B) Possible C-shaped cone (white arrow), or, alternatively a buried crater, located at 14.32°N, 303.10°E (NAC frame M135561817).

Table 1. Properties of Blocks Associated With Volcanic Landforms in the Marius Hills Region

Landform	Cone Summits	Distal Ends of Lobate Lava Flows
Diameter Minimum	1.3	1.0
Diameter Maximum	28	9.2
Diameter Average	3.0	2.4
Diameter std. dev.	1.3	0.7
Population b-slope	−3.8	−5.7
n	3054	3786
TOTAL		**6840**

3.3. Diviner Bulk Composition

[53] Diviner has three spectral bandpass filters centered at 7.8, 8.25, and 8.55 μm (Channels 3–5) and designed to characterize the position and shape of the Christiansen Feature (CF) [*Paige et al.*, 2010]. The CF is the mid-infrared emissivity maximum that occurs at wavelengths just shortward of the fundamental vibrational bands and is correlated with silicate polymerization, shifting to shorter wavelengths for felsic and feldspathic compositions and longer wavelengths for mafic compositions [*Conel*, 1969; *Logan et al.*, 1973; *Salisbury and Walter*, 1989]. Diviner is therefore directly
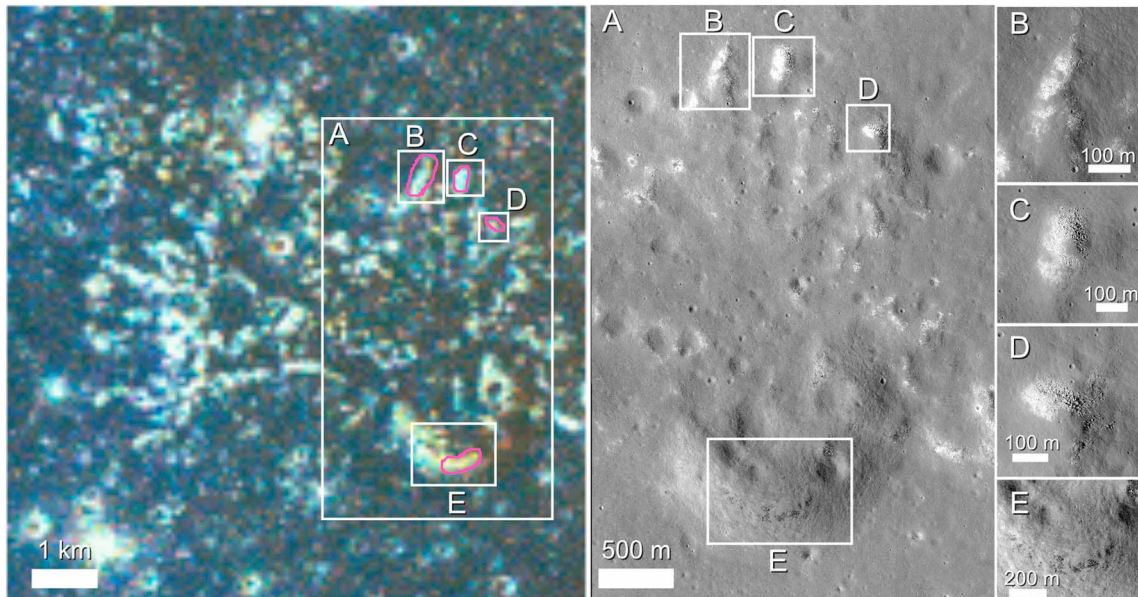
Figure 13. Mini-RF *m-chi* parameter map, where yellow and red areas represent locations of enhanced double backscatter and correlate to block regions in (A) LROC NAC frames. Inset boxes denote the block abundance count regions in this study; average CPR values in Table 2 calculated from pink outlined areas. Insets (B–D) are the distal ends of lava flows; inset (E) is the summit of a C-class cone.

Table 2. Radar and Physical Properties of Regions in Figure 13

Study Area	Minimum Block Size (m)	Maximum Block Size (m)	Mean Block Size (m)	Std. Dev. (m)	b	Average CPR
B	1.56	5.38	2.53	0.54	−5.41	0.62 ± 0.19
C	1.625	6.49	2.79	0.72	−5.30	0.62 ± 0.25
D	1.87	5.31	2.66	0.63	−5.23	0.80 ± 0.25
E	1.67	10.95	3.39	1.62	−3.49	1.05 ± 0.28

sensitive to silicate mineralogy and the bulk SiO_2 content [*Greenhagen et al.*, 2010].

[54] Analyses of the Diviner CF and concavity maps for the Marius Hills region (Figure 14) reveal that none of the volcanic constructs in the region display either the short wavelength CF position or the concave-up spectral shape in this parameter space characterizes silica-rich lithologies like the Gruithuisen and Mairan domes [*Glotch et al.*, 2010, 2011]. The average CF position of the volcanic domes in the Marius Hills region is 8.30 ± 0.03 μm; these values are not significantly different from the average CF position of the typical basaltic maria, which is 8.30 μm [*Greenhagen et al.*, 2010]. Therefore, the Marius Hills are not enriched in silica relative to the surrounding mare units, consistent with previous observations from Clementine [*Weitz and Head*, 1999; *Heather et al.*, 2003].

4. Discussion

[55] The observed changes in slope along the flanks of the Marius Hills domes were first explained as increasing viscosity due to increasing silica content [*McCauley*, 1967a]. However, the Diviner CF and concavity data are not consistent with silica-rich compositions, such as those found at the Gruithuisen domes. Therefore, the changes in slope along the flanks of the domes and the steep (~16°), thick (≳30 m) lava flows found on many of the domes are better explained by changes in effusion rate, temperature, and/or crystallization as proposed by *Whitford-Stark and Head* [1977] and *Weitz and Head* [1999]. The steep portions of the domes correlate to thick, lobate lava flows. As indicated by NAC block populations, Diviner rock abundances, and Mini-RF backscattering ratios, these lava flows are blockier and rougher than the basaltic mare. This roughness was previously suggested by *Head and Gifford* [1980] and *Campbell et al.* [2009]. Changes in roughness of terrestrial basaltic lavas (e.g., Hawaiian pahoehoe to `a`a transitions or Icelandic blocky lavas) can result from changes in flow rate or temperature [*Head et al.*, 1978; *Peterson and Tilling*, 1980; *Cashman et al.*, 1999]. The larger overall size (up to 28 m) of blocks located on portions of the cones indicates that they might have originated from a coherent layer of lava, whereas the smaller overall size of blocks found on the ends of the lava flows might indicate that the surface was more fractured, more mechanically degraded, or less coherent as would be expected in a flowing lava. The blocks observed on many of the cones are typically found adjacent to in situ layers displaying joints or fracturing on a similar scale, implying that many of the blocks on the cones are derived from these layers. Furthermore, layers or fracturing are not evident at the distal ends of the Marius Hills lava flows, meaning that these block populations could represent `a`a-like vitrified or partially crystalline masses (clinkers),

blocky pile-ups, or remnants of the original rough texture of the lava flows.

[56] We have observed that some of these blocky lava flows originate from the central vents of small (0.5–2 km diameter) volcanic cones. These cones have relatively smooth and steep sides (up to 16°) with occasional boulder clusters or fractured outcrops of layered material. These cones are similar in size and morphology to terrestrial cinder cones (as noted above) and have been previously suggested as late-stage pyroclastic or spatter cones [*McCauley*, 1967a; *Whitford-Stark and Head*, 1977; *Weitz and Head*, 1999; *Heather et al.*, 2003]. Some of the cones are associated with lower-reflectance "dark" and/or "red" spots in Clementine multispectral band ratio images that are distinct from the surrounding mare [*Weitz and Head*, 1999; *Heather et al.*, 2003]. The C-class cones have the best geographic correlation to these spectral anomalies and reduced albedo. *Heather et al.* [2003] and *Weitz and Head* [1999] have suggested that a glassy texture could explain the Clementine band ratios, and preliminary M^3 results also indicate the possible presence of either glassy materials or opaques correlated with these "dark" spots [*Besse et al.*, 2011]. The composition of the cones inferred from the spectral properties revealed by Clementine and M^3 observations might indicate that the cones represent late-stage volcanic eruptions. At least some of the dome-building flows originate directly from the C-shaped vents, indicating that cone formation can occur during dome construction, and perhaps both the lobate lava flows and volcanic cones were formed simultaneously during the last stages of regional volcanism when effusion rates and/or temperatures would be lower and the viscosity higher. The spectral differences between the "dark and/or red spot" cones could therefore plausibly be accounted for by the physical properties of the emplaced materials, such as particle size effects or the quenching of eruptive materials near the source vent, while more insulated materials, represented by layers in the cone walls, were able to intermittently flow out through breaches in the cone walls.

4.1. Cone Morphology and Formation

[57] Volcanic cones are generally constructed from near-vent lava and/or pyroclastic materials. Pyroclastic materials when ejected can have a range of sizes and will be liquid or solid when they land depending on their composition, temperature, particle size, and the time of flight. For terrestrial basaltic eruptions, the ultimate shape of the cone depends primarily on effusion rate, gas content, ballistic distribution of particles, and mass wasting [*McGetchin et al.*, 1974; *Settle*, 1979; *Head and Wilson*, 1989].

[58] Terrestrial cinder cones are constructed primarily from pyroclastics that have cooled enough to be solid when they land [*Head and Wilson*, 1989]. The size and shape of a cinder cone can be influenced by the volume of magma erupted, ejecta velocity and angle, size of particles,
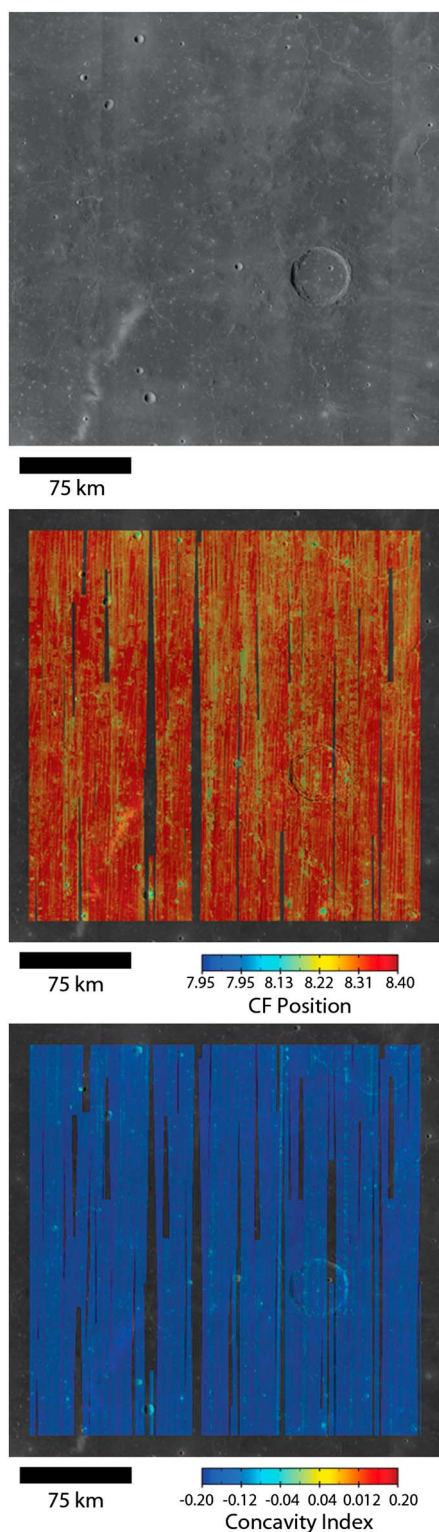
Figure 14. (a) LROC WAC base map of the Marius Hills region. (b) Christiansen Frequency (CF) location map for the Marius Hills region overlaid on LROC WAC morphology base map. In this parameter space, blue tones have low CF values and red tones have high CF values. (c) Diviner Concavity Index map for the Marius Hills region overlaid on LROC WAC morphology base map. Silicic compositions would be indicated by high values of the index (red). Note lack of red values.

subsequent lava flows, and vent geometry and spacing [e.g., *Settle*, 1979; *Wilson and Head*, 1981; *Wood*, 1979]. The C-class cones in the Marius Hills are typically 0.5–2 km in diameter and are comparable to the dimensions of terrestrial cinder cones, which may be a few hundred meters to 2.5 km in diameter [*Wood*, 1979; *Wilson and Head*, 1981].

[59] In terrestrial occurrences, lava flows are commonly associated with cinder cones [e.g., *Wilson and Head*, 1981; *Wood*, 1979, 1980]. Spatter cones, however, are constructs consisting of pyroclasts that were partly or completely molten when they landed but the eruption rate was too low for flows to form, allowing material to build up at the vent to form a cone-shaped construct [e.g., *Head and Wilson*, 1989]. Slopes of terrestrial spatter cones can be greater than the angle of repose (>30°) but diameters are typically less than cinder cones [*Porter*, 1972; *Wood*, 1979]. Terrestrial composite cones are constructed from interbedded pyroclasts and lava flows and have lower slopes than cinder and spatter cones.

[60] The flank slopes of the Marius Hills cones are lower than those of terrestrial cinder cones of the same diameter. Differences in diameter, heights, and slopes due to the several billion year age of the Marius Hills cones might be expected when compared to fresh terrestrial cones. However, *Wood* [1980] found little change in overall terrestrial cinder cone flank slopes with degradation because terrestrial cinder cone flanks usually form at or near the angle of repose. Models by *McGetchin and Head* [1973] suggest that lunar pyroclastic eruptions should form very low and broad features rather than cones due to lower gravity and lack of atmosphere. Models of *Wilson and Head* [1981] and *Whitford-Stark and Head* [1977] demonstrate that while lunar cinder and spatter cones can form from larger pyroclastic particles, these constructs should have lower flank slopes due to wider dispersal of pyroclastics, a result that is consistent with our slope measurements of ≤16°. These lower slopes may be typical of lunar volcanic cinder cones, where slopes do not reach the angle of repose. However, the layers observed in many of the C-class cones are coherent and have aligned blocks that we interpret to represent the original volcanic stratigraphy of the cone (Figure 7), suggesting that many of the Marius Hills cones are not simply composed of pyroclastic (cinder) material.

[61] Furthermore, the observed layering implies variable eruption conditions over time, similar to those suggested for Rima Parry V by *Head and Wilson* [1993]. The additional variability of layering, size, and shape from cone to cone reflects diverse constructions from cinder, spatter, and/or lava flows, and these changes in eruption conditions may also explain the lower slopes of the Marius Hills cones. Based on the similarities in general morphology and structure to terrestrial cinder cones, the Marius Hills C-class, E-class, and N-class cones are therefore considered to be volcanic constructs composed primarily of cinder and/or spatter with or without a lesser component of lava.

[62] The unique shape of the C-class cones has resulted from either asymmetrical construction or an initially symmetrical cone that was later disrupted to form the current morphology. Breached terrestrial cinder cones commonly result from an asymmetric distribution of pyroclastic material primarily due to the prevailing wind direction [e.g.,

Porter, 1972]; however, on the Moon, the observed asymmetry of C-class cones must be explained by a different mechanism. Likely scenarios include (1) the non-uniform eruption and emplacement of pyroclastics and lava around the vent resulting in asymmetrical construction of the rim; (2) pre-existing topography directs erupting lavas away from the vent in the downslope direction and prevents the construction of the downslope wall, resulting in an asymmetrical cone; (3) a directional weakness formed in a symmetrical cone due to a pileup of lava and/or pyroclastics on one side results in the collapse of one wall of the cone and is accompanied by a breakout of lava from the cone wall [i.e., *Harwood*, 1989]; and/or (4) pre-existing topography controls the flow direction of erupting lavas and results in the destruction of the downslope rim through thermal erosion.

[63] We observe that the point of highest topography along the rim of a C-class cone is roughly opposite the gap formed by lava leaving the vent area, inconsistent with a cone that was initially symmetric. Figure 8 shows that the direction of C-class cone breaching often coincides with the local topographic gradient, suggesting that formation of the C-class cones could be driven, at least in part, by pre-existing topography. This mechanism has recently been considered in terrestrial cinder-cone construction when prevailing winds could not adequately explain cone shapes [e.g., *Corazzato and Tibaldi*, 2006; *Sutawidjaja and Sukhyar*, 2009]. On Mauna Kea, Hawaii, flows commonly emerge from the downslope side of cinder cones [*Porter*, 1972]. Therefore, the Marius Hills C-class cones might have formed when flows (1) overtopped the rim at the lowest, most downslope point, eroded the cone wall, and formed the final shape, (2) the breach occurred when molten lava accumulated and exerted more pressure on the downslope wall causing a wall failure accompanied by an effusion of lava, or (3) erupting lavas followed pre-existing topography preventing formation of a downslope wall. In any case, lava would continue to drain through the resulting breach until eruptions waned, prohibiting formation of a new wall. Alternatively, pyroclasts and lava may not have been deposited symmetrically, possibly due to partial clogging of the vent [e.g., *Porter*, 1972].

[64] N-class cones, which are less abundant but are more symmetric than the C-class and E-class cones, provide some evidence for a symmetrical formation method. In this case, the cones begin symmetrical and through a breaching event become asymmetrical. Alternatively, N-class cones may represent areas where lava effusions were less abundant or were not as strongly affected by pre-existing topography. The elongate morphology of the E-class cones suggests formation along a fissure eruption, as was originally suggested by *Greeley* [1971].

[65] In the Marius Hills, cones are sometimes observed in groups or alignments (Figure 9). Breaches in grouped cones can occur in different directions and are not always in alignment with regional topographic contours. This orientation of breaches may be due to local topography and/or "obstacle" effects created by the neighboring cones. In terrestrial cinder-cone fields, cone diameter is related to the distance between cones, where smaller cones form at shorter distances, and spatial distribution and alignment can provide subsurface structural information [*Settle*, 1979]. At Mauna Kea, for example, some cinder cones are arranged along

fracture zones and can occur in small groups [*Porter*, 1972]. Therefore, the clusters of cones in the Marius Hills could result from a variety of factors that concentrate the magma supply in certain locations. Such factors include dense concentrations of near-surface dikes [*Head and Wilson*, 1993], subsurface fractures [*Porter*, 1972; *Corazzato and Tibaldi*, 2006; *Sutawidjaja and Sukhyar*, 2009], and/or the migration of lava along a slope [*Porter*, 1972; *Sutawidjaja and Sukhyar*, 2009].
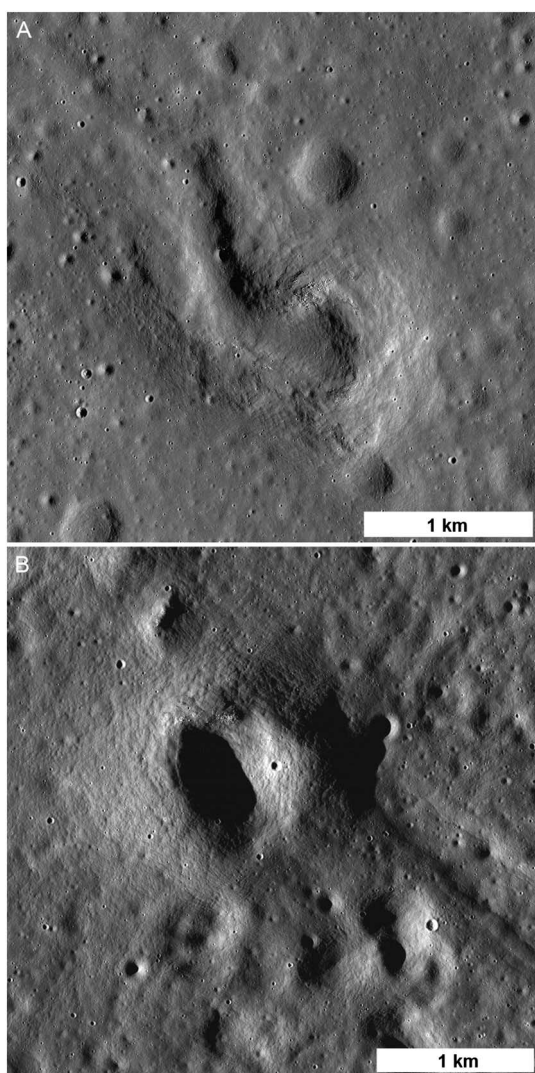
4.2. Regional Volcanism

[66] The physical characteristics and morphometry of lava flows provide insight into eruption conditions [*Peterson and Tilling*, 1980; *Wilson and Head*, 1994]. Some lava flows associated with the Marius Hill**s** cones and vents are on the order of 2 to 4 km long, often radiate from the cone, and have lobate margins with distinct slopes. Fresh boulders exposed in these slopes help to identify individual flow lobes in images and data products. Lava flows result in an undulating appearance (Figures 2 and 3). Pre-existing topography affects terrestrial lava flow morphology, and in certain situations steep slopes can result in clinkers and rubble [*Walker*, 1967; *Walker et al.*, 1973]. Conversely, pre-existing depressions can act as hosts allowing lava to pond.

[67] *Takeda et al.* [1975] used X-ray single-crystal diffraction studies and pyroxene thermobarometry of returned *Apollo 12* and *Apollo 15* mare basalt samples to show that those samples were derived from lava flows with thicknesses of 10 m or less. More recently, LROC NAC observations of layering in pits in the mare near Marius Hills suggest that the thicknesses of some individual mare flow layers in this region are 3–14 m [*Robinson et al.*, 2012]. Our measurements collected from LROC NAC-derived DEMs indicate that lobate flows associated with the Marius Hills domes have thicknesses of 30–90 m, making them significantly thicker than the known thicknesses of a typical mare basalt flow.

[68] The lengths and thicknesses of the lava flows alone may not be enough to differentiate between mafic and silicic compositions because of the fact that while higher viscosity lavas can form thicker and shorter flows, lava flows of different viscosities can have similar flow lengths [e.g., *Walker et al.*, 1973]. Previous spectroscopic investigations using Clementine and M^3 data sets have shown that the Marius Hills domes are not distinct in terms of iron or titanium content from the surrounding mare [*Weitz and Head*, 1999; *Heather et al.*, 2003; *Besse et al.*, 2011]. Thus, the new LRO morphology data combined with Clementine, M^3, and Diviner compositional data suggest that the shorter length and greater thickness of the lobate Marius Hills lava flows compared to a more typical mare indicate that the Marius Hills domes are a relatively more viscous but still non-silicic composition erupted either at a lower rate, lower temperature, and/or with a greater fraction of crystals.

4.2.1. Depressions and Collapse Features

[69] In addition to cones, some of the domes in the Marius Hills have sub-circular to elongate depressions, often called rimless depressions, on their flanks which are possible products of magma withdrawal, sinuous rille formation, or gravity slumping (e.g., Figure 2a). A survey of these rimless depressions using LROC data indicates that they are found throughout the Marius Hills region on a variety of scales

Figure 15. Other lunar volcanic constructs similar in morphology to Marius Hills cones. (A) Isis, a 1.5 km diameter breached volcanic cone in Mare Serenitatis located at 18.96°N, 27.48°E (NAC frame M146804182). (B) Osiris, a 1.9 km diameter volcanic cone in Mare Serenitatis located at 18.65°N, 27.65°E (NAC frame M101978309).

elsewhere on the Moon. For example, Isis, located in Mare Serenitatis (18.96°N, 27.48°E), is a 1.5 km diameter cone that is also C-shaped, smooth-sided, and has a gap and a lava channel (Figure 15a). Topographic data produced from Apollo 17 orbital photography indicate that Isis is roughly 70 m in height and has an exterior slope of 7.1° [*Weitz and Head*, 1999]. This feature is similar in morphology to some Marius Hills cones. Like many volcanic constructs in mare regions, Isis is embayed by younger mare, which may conceal some of its structure. The Isis cone is also proximal to a linear rille that is also suggested to be involved in its formation [*Scott*, 1973; *Wilson and Head*, 1996; *Weitz and Head*, 1999]. Osiris (Figure 15b) is another similar volcanic construct ~1.9 km in diameter, located southeast of Isis (18.6°N, 27.6°E). However, Osiris is a more symmetrical cone and does not have a gap in the cone wall. This feature is roughly 90 m high, and has an exterior slope of 7° [*Weitz and Head*, 1999]. Both of these cones are similar in diameter to the cones of the Marius Hills, but have lower reported slopes, which may be a function of the available topographic data. A NAC DEM was not available at the time of publication to compare the morphology of Isis and Osiris at the meter scale to the cones of the Marius Hills.

[71] Relationships between summit crater diameter and base diameter of volcanic constructs can be used to distinguish other volcanic constructs from cinder cones, which are smaller but have relatively larger summit craters [e.g., *Pike*, 1978; *Smith*, 1973; *Wood*, 1979]. Figure 16 compares the summit diameters to the base diameters for Marius Hills cones. The summit diameters of the Marius Hills cones are calculated as average values and exclude any breached areas. *Porter* [1972] and *Wood* [1980] observed a summit diameter to base diameter (D_S/D_B) ratio of 0.4 for fresh terrestrial cinder cones. *Wood* [1979, and references therein] reported D_S/D_B ratios of 0.36 for terrestrial spatter cones, 0.08 for terrestrial low shield volcanoes, and 0.12 for steep terrestrial shield volcanoes. *Smith* [1973] reported D_S/D_B ratios of 0.4–0.7 for high viscosity terrestrial lava domes and 0.05–0.2 for terrestrial stratovolcanoes and shield volcanoes. The D_S/D_B ratio reflects particle size, width of vent, gas content, eruption rate, constancy of eruption, and any crater collapse [*Head*, 1975; *Wood*, 1979; *Head and Gifford*, 1980; *Wilson and Head*, 1981]. The average $D_S/$
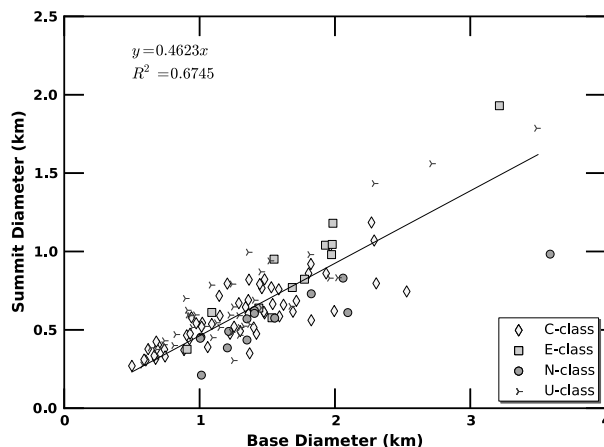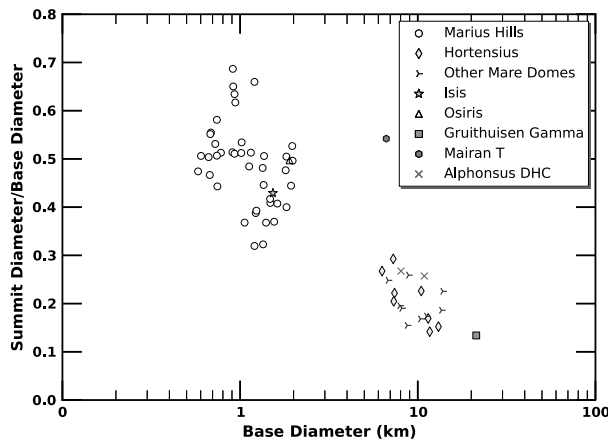
from less than 1 km wide to several kilometers in length and are commonly associated with partially obscured sinuous or linear rilles. *Weitz and Head* [1999] hypothesized that some of the larger topographic depressions most likely formed by collapse after magma withdrawal at depth. *Greeley* [1971] illustrated a relationship between depressions and the source vents of sinuous rilles. Some of these depressions in the Marius Hills are related to, or found in, chains and these may be related to the partial collapse of lava tubes [*Greeley*, 1971].

4.3. Comparison to Other Lunar Features

[70] As shown in Figure 4, the Marius Hills complex contains volcanic constructs unique in morphology compared to other regions [e.g., *Head and Gifford*, 1980], but there are several recognized volcanic cones similar in size and shape to the cones located in the Marius Hills region

Figure 16. Base diameter and summit diameter of Marius Hills cones and possible cones.

Figure 17. Summit diameter and base diameter of selected Marius Hills cones and other lunar volcanic constructs. Lunar cones have a distinct D_S/D_B compared to other lunar features. Marius Hills domes are not included because they do not have summit craters.

D_B ratio is 0.48 for the cones in the Marius Hills and ranges from 0.21 to 0.78. The Marius Hills D_S/D_B ratio is close to that of terrestrial cinder cones, as previously noted by *Wood* [1979], but is also similar to that of high viscosity lava domes. The D_S/D_B ratios for Marius Hills cones reflects either a slightly larger diameter summit crater relative to the base compared to terrestrial cinder cones or may reflect the more viscous nature of the eruptions associated with the lobate lava flows. The range of values indicates variability in eruption conditions, consistent with the irregular morphologies observed in many of the domes and cones.

[72] The Marius Hills cones have D_S/D_B ratios similar to Isis and Osiris, suggesting that these features formed from similar eruption conditions (Figure 17). The D_S/D_B ratios were determined from NAC images that were processed in the same manner as those used at Marius Hills. Unlike the Marius Hills cones, however, Isis and Osiris appear to be the only such features in that part of Mare Serenitatis. The Marius Hills cones have smaller base diameters and larger D_S/D_B ratios, when compared to other lunar volcanic constructs including mare domes, such as Hortensius, Tobias Meyer, Milichius, Grace, and Diana, Alphonsus-type dark halo craters, and non-mare domes including Mairan T and Gruithuisen Gamma, consistent with preliminary results of *Wood* [1979]. The difference in D_S/D_B suggests a different style of volcanism has occurred in the Marius Hills compared to that of other lunar domes and cones, specifically, localized effusions of relatively viscous materials not enriched in silica compared to the surrounding mare basalts.

5. Conclusions

[73] Over 150 volcanic domes and 90 cones in the Marius Hills have been identified and characterized using new Lunar Reconnaissance Orbiter Camera observations. The volcanic cones are classified into separate morphological categories: C-class (C-shaped), E-class (elongate), and N-class (no gap). The total number of probable kilometer-scale volcanic cones (n = 93) identified in this study is roughly twice previously reported numbers.

[74] Overall, the changes in slope along the flanks of the domes are best explained by changes in viscosity due to effusion rate, temperature, and or degree of crystallization. The steep (~16°) portions of the domes correlate to thick (>30 m) lobate blocky lava flows. Block sizes, rock abundances, and radar backscattering indicate that these lava flows are blockier and rougher than the surrounding and younger mare.

[75] Some of these lava flows have small C-shaped cones, 0.5–2 km in diameter, as their source. These cones have relatively smooth and steep sides (~16°) with occasional clusters of boulders found weathering out of layered outcrops. These cones are comparable in morphology (slope, diameter, and D_s/D_B ratios) to terrestrial cinder cones, although their slopes are less than the angle of repose. Layering in some cones, combined with lower slopes, is consistent with varying amounts of cinder, spatter, and lava.

[76] The wide range of D_S/D_B ratios is further consistent with the irregular shapes and morphologies of domes and cones throughout the Marius Hills. The blocks associated with portions of the cones are larger than blocks found at the ends of the lobate lava flows, suggesting the blocks on the cones are derived from a coherent layer of lava, whereas the smaller blocks of the lava flows may be derived from a more fractured, less coherent material resulting from flowing lava. Layers and fracturing are not observed at the ends of the lava flows, consistent with these being largely piles of blocks or clinkers.

[77] The gap present in the C-class cones strongly resembles the breaches in terrestrial cinder cones. Analysis of the C-class volcanic cones indicates that the morphology of the Marius Hills cones (in particular, the orientation of the gaps) was controlled, at least in part, by local topography and lava eruptions. The Marius Hills C-class cones, therefore, might have acquired their distinct shape when flows overtopped the rim at the lowest point and eroded the cone walls, when the cone was breached where lava accumulated at the lowest point, or as flows followed pre-existing slopes preventing the formation of the downslope wall. The less common N-class cones have poorly defined gaps and may represent cones where pre-existing topography and lava eruptions had less influence. The elongate shapes of the E-class cones are indicative of fissure-style eruptions. Some cones are aligned into groups or clusters and may represent areas of magma concentrations. In addition, there are numerous irregularly shaped features in the Marius Hills that may be degraded cones.

[78] Comparisons between LROC, Mini-RF, and Diviner observations confirm that volcanic domes in the Marius Hills are composed of rough, blocky lava flows which are not enhanced in silica relative to the surrounding mare basalts. The basaltic lava flows that make up volcanic domes in the Marius Hills region are thicker and shorter than surrounding mare basalt flows, suggesting lower effusion rates coupled with increased viscosity as might be expected during late-stage eruptions. NAC observations indicate that some of the dome-building flows originate from the C-class vents, suggesting that cones form during dome-building, and perhaps the lobate lava flows and volcanic cones formed synchronously during the last stages of volcanism in the Marius Hills region. The layers in the cone walls represent the intermittent effusions of lava and variable eruption

conditions during terminal volcanism and correlate to the thick, lobate flows observed on many of the domes. The variability of layering from cone to cone further reflects the diverse eruption conditions ranging from cinder, spatter, and/or lava flows resulting in the formation of Marius Hills cones. Overall, the volcanic history of the Marius Hills is complex, and domes and cones represent a variety of eruption styles.

[79] The early hypotheses of McCauley [1967b] that low domes are formed by laccoliths, that steep domes and rough lava flows are produced by later viscous eruptions, and that the cones are formed by late-stage pyroclastics, do account for the general morphologic variations observed in the domes and cones of the Marius Hills. The morphologies and relationships observed in this study are consistent with multistage eruptions resulting in different morphologies. The low domes could be either eroded lava flows or formed by intrusions. The steep-sided lava flows are directly related to many cones and may have formed contemporaneously as accumulations of pyroclastics and lava near the vent. However, contrary to McCauley's early hypothesis, and consistent with later hypotheses [*Weitz and Head*, 1999; *Heather et al*., 2003], we find that instead of a more silicic composition, the observed changes in morphology and the lack of spectral differences between the steep-sided Marius Hills lava flows and the surrounding mare in both Clementine and Diviner spectral data are more consistent with variations in volcanic style due to changes in effusion rate, crystallinity, and/or magma temperature over time. Variable eruption rates can account for differential layering and the different cone morphologies (i.e., breached and unbreached). Eruptions along fissures or fault lines could account for localized groupings, cone alignments, and elongated cone morphologies.

References

Anderson, S. W., E. R. Stofan, J. J. Plaut, and D. A. Crown (1998), Block size distributions on silicic lava flow surfaces: Implications for emplacement conditions, *Geol. Soc. Am. Bull.*, *110*(10), 1258–1267, doi:10.1130/0016-7606(1998)110<1258:BSDOSL>2.3.CO;2.

Bandfield, J. L. (2009), Effects of surface roughness and graybody emissivity on Martian thermal infrared spectra, *Icarus*, *202*, 414–428, doi:10.1016/j.icarus.2009.03.031.

Bandfield, J. L., and C. S. Edwards (2008), Derivation of Martian surface slope characteristics from directional thermal infrared radiometry, *Icarus*, *193*, 139–157, doi:10.1016/j.icarus.2007.08.028.

Bandfield, J. L., R. R. Ghent, A. R. Vasavada, D. A. Paige, S. J. Lawrence, and M. S. Robinson (2011), Lunar surface rock abundance and regolith fines temperatures derived from LRO Diviner Radiometer data, *J. Geophys. Res.*, *116*, 18, doi:10.1029/2011JE003866.

Besse, S., J. M. Sunshine, M. I. Staid, N. E. Petro, J. W. Boardman, R. O. Green, J. W. Head, P. J. Isaacson, J. F. Mustard, and C. M. Pieters (2011), Compositional variability of the Marius Hills volcanic complex from the Moon Mineralogy Mapper (M3), *J. Geophys. Res.*, *116*, 15, doi:10.1029/2010JE003725.

Bussey, D. B. J., et al. (2010), Initial Results from Mini-RF: A synthetic aperture radar on Lunar Reconnaissance Orbiter, in *Lun. Plan. Sci. Conf. 41*, p. 2319, Lunar and Planetary Institute, Houston, Tex.

Cahill, J. T. S., D. B. J. Bussey, G. W. Patterson, F. S. Turner, N. R. Lopez, R. K. Raney, C. D. Neish, and Mini-RF Team (2012), Global Mini-RF S-band CPR and m-chi decomposition observations of the Moon, in *Lun. Plan. Sci. Conf. 43*, p. 2590, Lunar and Planetary Institute, Houston, Tex.

Campbell, B. A., and D. B. Campbell (2006), Regolith properties in the south polar region of the Moon from 70-cm radar polarimetry, *Icarus*, *180*, 1–7, doi:10.1016/j.icarus.2005.08.018.

Campbell, B. A., B. R. Hawke, and D. B. Campbell (2009), Surface morphology of domes in the Marius Hills and Mons Rumker regions of the Moon from Earth-based radar data, *J. Geophys. Res.*, *114*, 01001, doi:10.1029/2008JE003253.

Cashman, K. V., C. Thornber, and J. P. Kauahikaua (1999), Cooling and crystallization of lava in open channels, and the transition of Pāhoehoe Lava to "A'ā, *Bull. Volcanol.*, *61*(5), 306–323, doi:10.1007/s004450050299.

Christensen, P. R. (1986), The spatial distribution of rocks on Mars, *Icarus*, *68*, 217–238, doi:10.1016/0019-1035(86)90020-5.

Cintala, M. J., J. B. Garvin, and S. J. Wetzel (1982), The distribution of blocks around a fresh lunar mare crater, in *Lunar and Planetary Science Conference Abstracts*, vol. 13, pp. 100–101, Lunar and Planetary Institute, Houston, Tex.

Colwell, J. E., and B. M. Jakosky (2002), Effects of topography on thermal infrared spectra of planetary surfaces, *J. Geophys. Res.*, *107*, 5106, doi:10.1029/2001JE001829.

Conel, J. E. (1969), Infrared emissivities of silicates: Experimental results and a cloudy atmosphere model of spectral emission from condensed particulate mediums, *J. Geophys. Res.*, *74*(6), 1614–1634, doi:10.1029/JB074i006p01614.

Corazzato, C., and A. Tibaldi (2006), Fracture control on type, morphology and distribution of parasitic volcanic cones: An example from Mt. Etna, Italy, *J. Volc. Geotherm. Res.*, *158*, 177–194, doi:10.1029/2008JE003253.

Elston, D., and C. Willingham (1969), Five day mission plan to investigate the geology of the Marius Hills region of the Moon, United States Geological Survey Interagency Report: Astrogeology 14, United States Geological Survey, Washington, D. C.

Garvin, J. B., P. J. Mouginis-Mark, and J. W. Head (1981), Characterization of rock populations on planetary surfaces—Techniques and a preliminary analysis of Mars and Venus, *Moon Planets*, *24*, 355–387.

Glotch, T. D., et al. (2010), Highly silicic compositions on the Moon, *Science*, *329*(5998), 1510–1513, doi:10.1126/science.1192148.

Glotch, T. D., J. J. Hagerty, P. G. Lucey, B. R. Hawke, T. A. Giguere, J. A. Arnold, J. P. Williams, B. L. Jolliff, and D. A. Paige (2011), The Mairan domes: Silicic volcanic constructs on the Moon, *Geophys. Res. Lett.*, *38*(21), L21204, doi:10.1029/2011GL049548.

Greeley, R. (1971), Lava tubes and channels in the lunar Marius Hills, *Moon*, *3*, 289–314.

Greenhagen, B. T., et al. (2010), Global silicate mineralogy of the Moon from the Diviner Lunar Radiometer, *Science*, *329*(5998), 1507–1509, doi:10.1126/science.1192196.

Gruener, J. E., and B. K. Joosten (2009), NASA Constellation Program Office Regions of Interest on the Moon: A representative basis for scientific exploration, resource potential, and mission operations, *LPI Contri.*, *1483*, 50–51.

Guest, J. E., and J. B. Murray (1976), Volcanic features of the nearside equatorial lunar maria, *J. Geol. Soc.*, *132*(3), 251–258, doi:10.1144/gsjgs.132.3.0251.

Hartmann, W. K. (1967), Secondary volcanic impact craters at Kapoho, Hawaii and comparisons with the lunar surface, *Icarus*, *7*(1-3), 66–75, doi:10.1016/0019-1035(67)90048-6.

Hartmann, W. K. (1969), Terrestrial, lunar, and interplanetary rock fragmentation, *Icarus*, *10*(2), 201–213, doi:10.1016/0019-1035(69)90022-0.

Harwood, R. D. (1989), Cinder cone breaching events at Strawberry and O'Neill craters, San Francisco volcanic field, Arizona, M. S. Thesis, Northern Arizona University, Flagstaff, Ariz.

Head, J. W. (1975), Morphology of pyroclastic lunar volcanic deposits: Implications for eruption conditions and localized sources of volatiles, in *Abstracts of the Lunar and Planetary Science Conference, Vol. 6*, p. 349, Pergamon Press, Houston, Tex.

Head, J. W., and A. Gifford (1980), Lunar mare domes—Classification and modes of origin, *Moon and Planets*, *22*, 235–258, doi:10.1007/BF00898434.

Head, J. W., and L. Wilson (1989), Basaltic pyroclastic eruptions: Influence of gas-release patterns and volume fluxes on fountain structure, and the formation of cinder cones, spatter cones, rootless flows, lava ponds and lava flows, *J. Volc. Geotherm. Res.*, *37*(3-4), 261–271, doi:10.1016/0377-0273(89)90083-8.

Head, J. W., and L. Wilson (1993), Lunar graben formation due to near-surface deformation accompanying dike emplacement, *Planet. Space Sci.*, *41*(10), 719–727, doi:10.1016/0032-0633(93)90114-H.

Head, J. W., P. C. Hess, and T. B. McCord (1978), Geologic characteristics of lunar highland volcanic domes (Gruithuisen and Mairan Region) and

possible eruption conditions, Lunar and Planetary Science Conference Abstracts, vol. 9, pp. 488–490, Lunar and Planetary Institute, Houston, Tex.

Heather, D. J., and S. K. Dunkin (2002), A stratigraphic study of southern Oceanus Procellarum using Clementine multispectral data, *Planet. Space Sci.*, *50*(14-15), 1299–1309, doi:10.1016/S0032-0633(02)00124-1.

Heather, D. J., S. K. Dunkin, and L. Wilson (2003), Volcanism on the Marius Hills plateau: Observational analyses using Clementine multispectral data, *J. Geophys. Res.*, *108*, 5017, doi:10.1029/2002JE001938.

Jolliff, B. L. (2011), Non-mare silicic volcanism on the lunar farside at Compton-Belkovich, *Nature Geosci.*, *4*(8), 566–571, doi:10.1038/ngeo1212.

Karlstrom, T. N. V., J. F. McCauley, and G. A. Swann (1968), Preliminary lunar exploration plan of the Marius Hills region of the Moon, United States Geological Survey Interagency Report: Astrogeology 5, United States Geological Survey, Washington, D. C.

Lawrence, S. J., M. S. Robinson, B. L. Jolliff, E. Bowman-Cisneros, T. Tran, J. D. Stopar, B. R. Hawke, S. D. Thompson, S. Koeber, and LROC Targeting Action Team (2009), Preparing to scout the next frontier: Hardware and operational constraints encountered during targeting of the Lunar Reconnaissance Orbiter camera narrow angle cameras, in *Lun. Plan. Sci. Conf. 40*, p. 2316, Lunar and Planetary Institute, Houston, Tex.

Lawrence, S. J., et al. (2010a), LROC views the Constellation Regions of Interest: Science and exploration observations, in *LPI Contributions, Vol. 1595*, p. 35, Lunar and Planetary Institute, Washington, D. C.

Lawrence, S. J., J. D. Stopar, B. R. Hawke, L. R. Gaddis, M. S. Robinson, B. W. Denevi, T. A. Giguere, B. L. Jolliff, S. E. Braden, and LROC Team (2010b), LROC observations of the Marius Hills, in *Lun. Plan. Sci. Conf. 41*, p. 1906, Lunar and Planetary Institute, Houston, Tex.

Logan, L. M., G. R. Hunt, J. W. Salisbury, and S. R. Balsamo (1973), Compositional implications of Christiansen frequency maximums for infrared remote sensing applications, *J. Geophys. Res.*, *78*(23), 4983–5003, doi:10.1029/JB078i023p04983.

McCauley, J. F. (1967a), Geologic map of the Hevelius region of the Moon, *U. S. Geol. Surv. Misc. Invest. Ser.*, Map I-491, scale 1:1000000.

McCauley, J. F. (1967b), The nature of the lunar surface as determined by systematic geologic mapping, in *Mantles of the Earth and Terrestrial Planets*, edited by S. K. Runcorn, pp. 431–460, Interscience, New York.

McGetchin, T. R., and J. W. Head (1973), Lunar Cinder Cones, *Science*, *180*, 68–71.

McGetchin, T. R., M. Settle, and B. A. Chouet (1974), Cinder cone growth modeled after Northeast crater, Mount Etna, Sicily., *J. Geophys. Res.*, *79*, 3257–3272.

Neish, C. D., D. T. Blewett, D. B. J. Bussey, S. J. Lawrence, M. Mechtley, and B. J. Thomson (2011), The surficial nature of lunar swirls as revealed by the Mini-RF instrument, *Icarus*, *215*(1), 186–196, doi:10.1016/j.icarus.2011.06.037.

Nowicki, S. A., and P. R. Christensen (2007), Rock abundance on Mars from the Thermal Emission Spectrometer, *J. Geophys. Res.*, *112*, 05007, doi:10.1029/2006JE002798.

Nozette, S., et al. (2010), The Lunar Reconnaissance Orbiter Miniature Radio Frequency (Mini-RF) technology demonstration, *Space Sci. Rev.*, *150*(1-4), 285–302, doi:10.1007/s11214-009-9607-5.

Paige, D. A., et al. (2010), The Lunar Reconnaissance Orbiter Diviner Lunar radiometer experiment, *Space Sci. Rev.*, *150*(1-4), 125–160, doi:10.1007/s11214-009-9529-2.

Peterson, D. W., and R. I. Tilling (1980), Transition of basaltic lava from pahoehoe to aa, Kilauea Volcano, Hawaii: Field observations and key factors, *J. Volcanol. Geotherm. Res.*, *7*(3–4), 271–293, doi:10.1016/0377-0273(80)90033-5.

Pike, R. J. (1978), Volcanoes on the inner planets—Some preliminary comparisons of gross topography, in *Proc. Lun. Planet. Sci. Conf.*, vol. 9, pp. 3239–3273, New York, Pergamon Press, Houston, Tex.

Porter, S. (1972), Distribution, morphology, and size frequency of cinder cones on Mauna Kea Volcano, Hawaii, *Geol. Soc. Am. Bull.*, *83*(12), 3607–3612, doi:10.1130/0016-7606(1972)83[3607:DMASFO]2.0.CO;2.

Raney, R. K. (2006), Dual-polarized SAR and Stokes parameters, *IEEE Geosci. Remote Sens. Lett.*, *3*(3), 317–319, doi:10.1109/LGRS.2006.871746.

Raney, R. K., et al. (2010), The Lunar Mini-RF Radars: Hybrid polarimetric architecture and initial results, *Proc. IEEE*, *99*(5), 1–16, doi:10.1109/JPROC.2010.2084970.

Raney, R. K., J. T. S. Cahill, G. W. Patterson, D. B. J. Bussey, and Mini-RF Team (2012), The m-chi decomposition of hybrid dual-polarimetric radar data with application to lunar craters, *J. Geophys. Res.*, *In Press*, doi:10.1029/2011JE003986.

Robinson, M. S., J. W. Ashley, A. K. Boyd, R. V. Wagner, E. J. Speyerer, B. Ray Hawke, H. Hiesinger, and C. H. van der Bogert (2012), Confirmation of sublunarean voids and thin layering in mare deposits, *Planet. Space Sci.*, *69*(1), 18–27, doi:10.1016/j.pss.2012.05.008.

Robinson, M. S., et al. (2010), Lunar Reconnaissance Orbiter Camera (LROC) instrument overview, *Space Sci. Rev.*, *150*(1–4), 81–124, doi:10.1007/s11214-010-9634-2.

Salisbury, J. W., and L. S. Walter (1989), Thermal infrared (2.5–13.5 μm) spectroscopic remote sensing of igneous rock types on particulate planetary surfaces, *J. Geophys. Res.*, *94*(B7), 9192–9202, doi:10.1029/JB094iB07p09192.

Scholten, F., J. Oberst, K.-D. Matz, T. Roatsch, M. Wählisch, E. J. Speyerer, and M. S. Robinson (2012), GLD100: The near-global lunar 100 m raster DTM from LROC WAC stereo image data, *J. Geophys. Res.*, *117*, 12, doi:10.1029/2011JE003926.

Scott, D. H. (1973), Mare Serenitatis cinder cones and terrestrial analogs, in *Apollo 17 Preliminary Science Report*, pp. 30–7, NASA, Washington, D. C.

Settle, M. (1979), The structure and emplacement of cinder cone fields, *Am. J. Sci.*, *279*(10), 1089–1107, doi:10.2475/ajs.279.10.1089.

Smith, E. I. (1973), Identification, distribution and significance of lunar volcanic domes, *Moon*, *6*, 3–31.

Speyerer, E., M. Robinson, B. W. Denevi, and LROC Science Team (2011), Lunar Reconnaissance Orbiter camera global morphological map of the Moon, in *Lun. Plan. Sci. Conf. 42*, p. 2387, Lunar and Planetary Institute, Houston, Tex.

Sutawidjaja, I., and R. Sukhyar (2009), Cinder cones of Mount Slamet, Central Java, Indonesia, *J. Geol. Indonesia*, *4*(1), 57–75.

Takeda, H., M. Miyamoto, T. Ishii, and G. E. Lofgren (1975), Relative cooling rates of mare basalts at the Apollo 12 and 15 sites as estimated from pyroxene exsolution data, in *Proc. Lun. Plan. Sci. Conf.*, vol. 6, pp. 987–996, Pergamon Press and Lunar and Planetary Institute, Houston, Tex.

Tran, T., et al. (2010), Generating digital terrain models from LROC stereo images with SOCET SET, in *Lun. Plan. Sci. Conf. 41*, p. 2515, Lunar and Planetary Institute, Houston, Tex.

Walker, G. P. L. (1967), Thickness and viscosity of Etnean lavas, *Nature*, *213*(5075), 484–485, doi:10.1038/213484a0.

Walker, G. P. L., A. T. Huntingdon, A. T. Sanders, and J. L. Dinsdale (1973), Lengths of lava flows [and discussion], *Philos. Trans. R. Soc. London, Ser. A, Math. Phys. Sci.*, *274*(1238), 107–118.

Weitz, C. M., and J. W. Head (1999), Spectral properties of the Marius Hills volcanic complex and implications for the formation of lunar domes and cones, *J. Geophys. Res.*, *104*(E8), 18933–18956, doi:10.1029/1998JE000630.

Whitford-Stark, J. L., and J. W. Head (1977), The Procellarum volcanic complexes—Contrasting styles of volcanism, in *Proc. Lun. Plan. Sci. Conf., vol. 8*, pp. 2705–2724, Pergamon Press and Lunar and Planetary Institute, Houston, Tex.

Wilhelms, D. E. (1993), *To A Rocky Moon: A Geologist's History of Lunar Exploration*, pp. 260–283, University of Arizona Press, Tucson, Ariz.

Wilson, L., and J. W. Head (1981), Ascent and eruption of basaltic magma on the Earth and Moon, *J. Geophys. Res.*, *86*, 2971–3001, doi:10.1029/JB086iB04p02971.

Wilson, L., and J. W. Head (1994), Mars: Review and analysis of volcanic eruption theory and relationships to observed landforms, *Rev. Geophys.*, *32*, 221–263, doi:10.1029/94RG01113.

Wilson, L., and J. W. Head (1996), Lunar linear rilles as surface manifestations of dikes: Theoretical considerations, in *Lun. Plan. Sci. Conf. 27*, p. 1445, Lunar and Planetary Institute, Houston, Tex.

Wood, C. A. (1979), Monogenetic volcanoes of the terrestrial planets, in *Proc. Lun. Plan. Sci. Conf., vol. 10*, pp. 2815–2840, Lunar and Planetary Institute, Houston, Tex.

Wood, C. A. (1980), Morphometric analysis of cinder cone degradation, *J. Volc. Geotherm. Res.*, *8*(2–4), 137–160, doi:10.1016/0377-0273(80)90101-8.